TRIUMF

TECHNIQUES APPLIED TO THE DESIGN OF THE TRIUMF MAGNET POLES

S. Oraas

MESON FACILITY OF:

UNIVERSITY OF ALBERTA
SIMON FRASER UNIVERSITY
UNIVERSITY OF VICTORIA
UNIVERSITY OF BRITISH COLUMBIA

TRI-70-4

TRI-70-4

TRIUMF

TECHNIQUES APPLIED TO THE DESIGN OF THE TRIUMF MAGNET POLES

S. Oraas

This report is based on the author's thesis submitted to the Faculty of Graduate Studies of the University of British Columbia in partial fulfilment of the requirements for his MASc. degree - April 1970

Postal Address:

TRIUMF
University of British Columbia
Vancouver 8, B.C.
Canada

December 1970

ABSTRACT

This report presents some of the techniques used in designing the sector-focused magnet for the TRIUMF cyclotron. An empirical method is given for calculating the magnet pole tip shape required to contain a 500 MeV beam of H^- ions. The method is good only for small changes in the shape. In the test case, the generated pole tip had a spiral angle correct to within ±5 deg, and a hill angle correct to ±1 deg. The average field was found to be isochronous to ±70 G.

An empirical solution to the problem of finding the field inside the magnet air gap is also given. The magnetic field resulting from a given pole tip contour is calculated at a point on the median surface by finding the perpendicular distance from the point to the edge of the pole and comparing this to an experimentally measured curve of field against distance. Fields generated by this technique have their averages correct to within 70 G and flutter to within 8%. Again, previous knowledge of similar pole tips is assumed.

The method and results of calculating the pole edge position tolerances for the latest model magnet are given. The field strengths inside the steel return yoke as obtained from a series of flux measurements are also presented. Finally, it is shown that a simple approximation to the magnetic circuit of the magnet predicts the coil induction required to an accuracy of only 25%.

C O N T E N T S

LIST OF TABLES

LIST OF FIGURES

1. INTRODUCTION

The problem of designing a magnet which will produce a magnetic field capable of containing a beam of charged particles is a very difficult one. Present-day numerical techniques are not adequate to solve Maxwell's equations for the field inside a steel shape as complex as the TRIUMF magnet (see Figure 1), and hence different approaches must be used. Section 2 of this report is an attempt to calculate the pole geometry required to produce a cyclotron magnet. Section 3 is the reverse approach - given a magnet similar to the TRIUMF magnet, we can predict with some success the azimuthal field contours. Section 4 gives tolerances on the dimensions of the pole tip, as derived from the conditions necessary to produce a contained beam of H^- ions. Section 5 gives the results of the flux measurements on the TRIUMF model magnet, and it also shows that the simple equivalent magnetic circuit cannot be easily applied here.

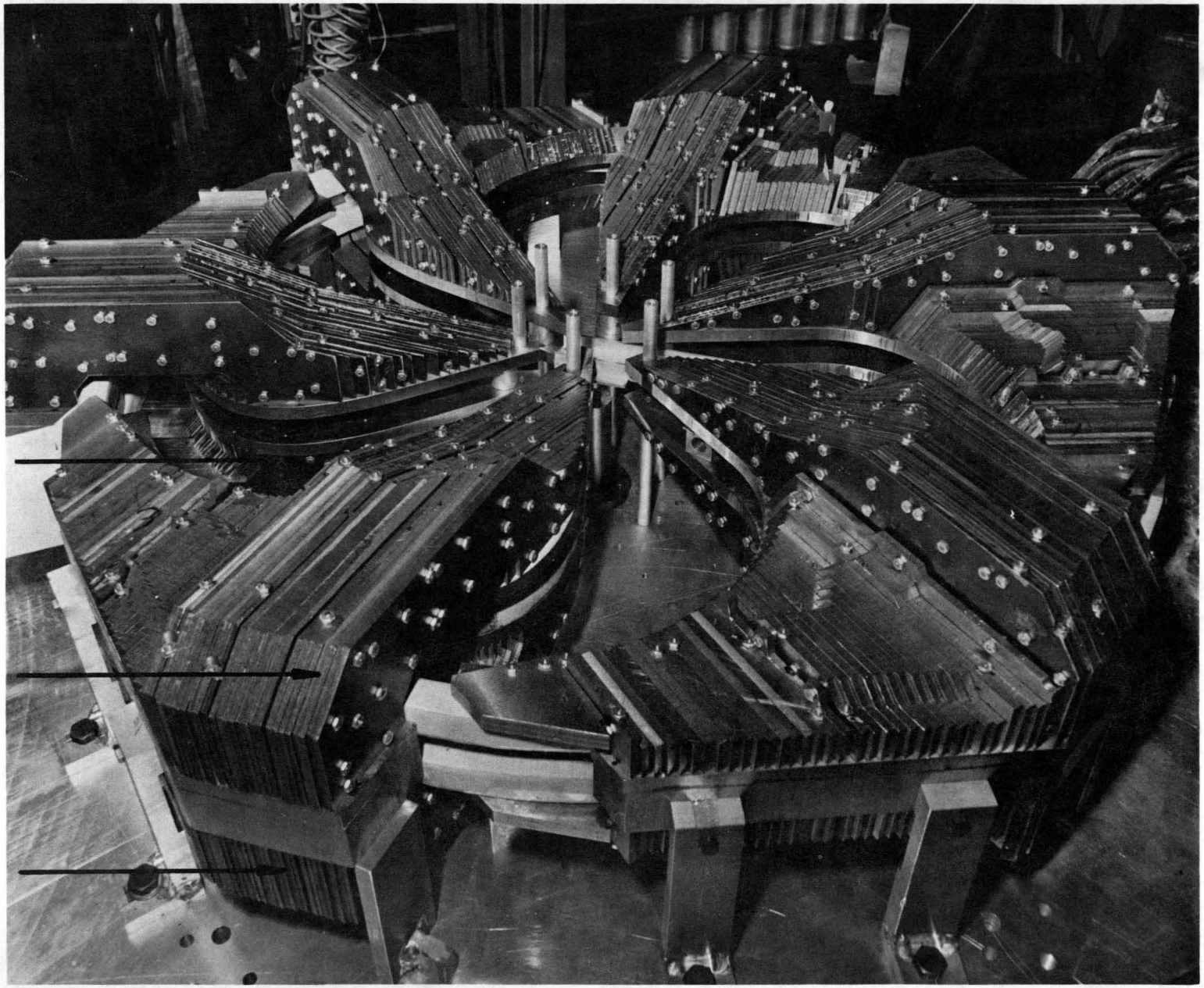

Figure 1. A photograph of the Mk VI-1 model magnet

2. POLE TIP DESIGN

2.1 Introduction

The method used for calculating the shape of a pole tip is basically that outlined in "Progress in Nuclear Techniques and Instrumentation", by J.R. Richardson,[1] with some modifications. The modifications are an attempt at applying second order corrections to the square wave approximation to the azimuthal field, taking into account the geometrical shape of the sectored magnet and the complex interdependence of the various design parameters. From the measurements done on the model magnets, these corrections were found to be reliable only for small changes in the pole tip shape.

2.2 Design Criteria

There are three conditions which must be met if a 500 MeV, 100 μA, CW H^- beam suitable for extraction from the cyclotron is to be produced. These are:

1) Isochronism
2) Focusing
3) Ion Lifetime

2.2.1 Isochronism

The isochronous condition requires that the ion must rotate at a constant angular velocity ω, and hence it defines the azimuthal average field required for any particle energy. We begin with the relativistic equations

$$\gamma \equiv \frac{E}{mc^2} = 1 + \frac{T}{mc^2} \tag{1}$$

and

$$\beta \equiv \frac{v}{c} = \sqrt{1 - \frac{1}{\gamma^2}} \tag{2}$$

where E = total energy of particle, T = kinetic energy, m = rest mass, v = velocity, and c = velocity of light. If we assume that the particle follows a circular orbit, we can use the equation for the Lorentz frequency of a particle with charge q in a magnetic field:

$$\omega = \frac{q\overline{B}}{\gamma m} = \text{constant for any cyclotron}$$

$$\text{or} \qquad \overline{B} = \frac{\omega\gamma m}{q} \tag{3}$$

where $\overline{B}$ is the field averaged over one revolution. This equation defines the isochronism condition. The central field, or the field required at zero particle energy, is

$$B_c = \frac{\omega m}{q} \tag{4}$$

from eqn. (3), letting $\gamma = 1$. The radius at which a particle of energy E orbits is determined from

$$\omega = \frac{v}{r} = \frac{\beta c}{r}.$$

$$\text{Thus} \qquad r = \frac{\beta c}{\omega}. \tag{5}$$

We can define the radius at which a particle of infinite energy would rotate:

$$r_\infty = \frac{c}{\omega}$$

from eqn. (5). From eqns. (3) and (4) we have

$$\frac{\overline{B}}{B_c} = \gamma = \frac{1}{\sqrt{1 - \beta^2}} \quad \frac{1}{\sqrt{1 - (r/r_\infty)^2}}. \tag{6}$$

The value of the orbiting frequency ω is set by design criteria 1) and 3).

2.2.2 Focusing

In order to achieve an adequate extraction efficiency, the beam must be focused radially and vertically. The radial condition is satisfied automatically, since for any many-sectored isochronous cyclotron such as TRIUMF, the number of radial betatron oscillations of the beam per turn is $\nu_r \approx \gamma$, and hence $\nu_r > 1.0$.[8] Thus the beam is contained

radially. The only real problem is to avoid resonances such as the $\nu_r = 1$ resonance, but this will affect only details of the magnet, not the overall general shape. Hence it will not be considered here.

Vertical focusing is more difficult to achieve. The radially increasing field required for isochronism produces a vertically defocusing force which must be compensated for by other properties of the magnet. Using the method of Smith and Garren,[2] we can express the radius of curvature $\mu(r,\theta)$ of the orbit in terms of a mixed Fourier and power series, as follows:

$$\mu(r,\theta) = \overline{\mu(r_0,\theta)} \left(1 + \mu' x + \mu'' \frac{x^2}{2} + \mu''' \frac{x^3}{6} + \ldots \right.$$
$$+ \sum_1^\infty (a_n \cos n\theta + b_n \sin n\theta)$$
$$+ x \sum_1^\infty (a_n' \cos n\theta + b_n' \sin n\theta)$$
$$\left. + \frac{x^2}{2} \sum_1^\infty (a_n'' \cos n\theta + b_n'' \sin n\theta) + \ldots \right) \quad (7)$$

where x is defined by $r = r_0(1 + x)$, r_0 is the radius at which the azimuthal average of μ is appropriate to the particle energy, i.e. $r_0 \overline{\mu(r_0,\theta)} = 1$, and a_n and b_n are the standard Fourier coefficients.

If we use this approximation to solve the equations of motion of the particle, we obtain the rather cumbersome expression for ν_z^2 given in appendix 2 of Smith and Garren. This equation cannot be easily reduced to a useful form by approximations which are valid for TRIUMF. Hence it was decided to try the reverse approach - choose an approximate formula and see how accurate it is. The formula chosen was the smooth approximation for ν_z^2, as given by Symen *et al.*,[11]

$$\nu_z^2 = -\mu' + F^2(1 + 2\tan^2\varepsilon) \quad (8)$$

where F^2 = "flutter" of field = $(\overline{B^2} - \overline{B}^2)/\overline{B}^2$, ε = spiral angle of field (see Figure 4), and $\mu' = \frac{r}{\overline{B}} \frac{\partial \overline{B}}{\partial r} = \beta^2\gamma^2$ if isochronism holds. This formula is comprised of a focusing and a defocusing term. The defocusing term, $-\mu'$, is due to the inward "bowing" of the field lines in the radially

increasing field required in a relativistic cyclotron. The focusing term $F^2(1 + 2\tan^2\varepsilon)$ is due to the three focusing forces arising from the spiral sector geometry of the magnet: the Thomas, alternating gradient, and Laslett forces.[8] At high energies, each of these two terms will be quite large, but the sum should be small and focusing. The limits on ν_z will be discussed in Section 4.1.

From equilibrium orbit programs such as CYCLOPS,[3] ν_z^2 can be determined within the necessary accuracy. Since F^2 is known for a given field, we can use eqn. (8) to calculate the spiral angle ε. The actual spiral angle of the field can be obtained directly from the Fourier harmonics of the field. If

$$B(\theta) = B + \sum_{n=1}^{\infty} A_n \sin(n\theta + \phi_n),$$

then $$\varepsilon_n = r\frac{d\phi_n}{dr}$$

where A_n is the amplitude of n^{th} harmonic, and ϕ_n and ε_n the phase and spiral angle of the n^{th} harmonic, respectively. The spiral angle ε of the field $B(\theta)$ can be found by applying the relation

$$\frac{1}{2}\sum_{n=0}^{\infty} A_n^2(1 + 2\tan^2\varepsilon_n) = F^2(1 + 2\tan^2\varepsilon).$$

Hence, by comparing the spiral angle obtained by eqn. (8) with the actual spiral angle of the field, we can estimate the accuracy of eqn. (8). The results from a typical model measurement are shown in Figure 2. It can be seen that for $R > 250$ in. the maximum deviation $\Delta\varepsilon$ from the two curves is ± 2 deg, and for $R < 150$ in., $\Delta\varepsilon = 14$ deg. These errors in ε can be translated into errors in ν_z^2 by the use of eqn. (8). The worst values of $\Delta\nu_z^2$ occur at $R = 150$ in. and $R = 305$ in., where $\Delta\nu_z^2 = \pm 0.022$ and ± 0.177, respectively. However, these numbers do not mean much by themselves. Since ν_z^2 is a difference of two relatively large numbers, we should consider $\Delta\nu_z^2$ as a percentage of either the focusing term or the defocusing term. We find that at both 150 in. and 305 in. radius $\Delta\nu_z^2 = \pm 14\%$. An error was to be expected because of the ignored terms in

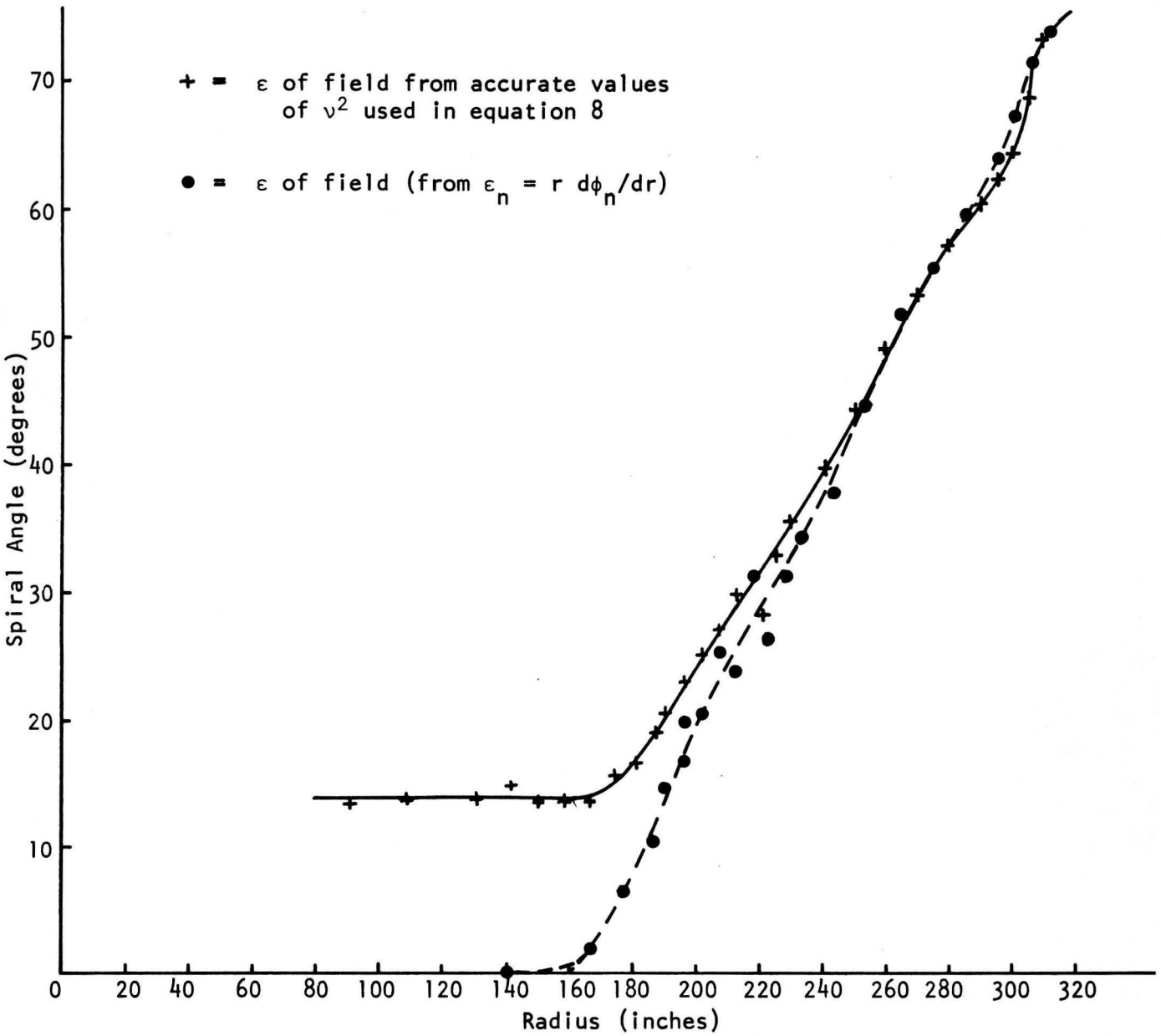

Figure 2. Spiral angle vs radius for the Mk VI-1 Mod 10 model magnet

the full expression for ν_z^2. These results give some confirmation that the approximations implicit in eqn. (8) are sufficiently valid that the use of such an equation and the use of model magnet measurements are adequate to design a sector-focused, isochronous magnet.

2.2.3 Ion Lifetime

Considerations such as radiation levels in the cyclotron vault and residual activity in the component parts of the cyclotron have led us to limit the allowable beam loss in TRIUMF to 10 kW. This means that the beam loss should be less than 20% of the extracted beam. There are two major causes of beam loss, both of which result from the very low binding energy of the extra electron in the H^- ion. First, the electron can be stripped by collision with gas molecules. This removes the charge of the ion, and since it will no longer be affected by the magnetic field, it will fly out of the machine. Hence we must have as low a gas pressure as possible in the vacuum tank. A pressure of 10^{-7} Torr was chosen for TRIUMF, as this is fairly easily achieved with present-day vacuum technology, and it results in a 4.6% beam power loss.[4]

The electrons can also be stripped by the electric field which results from the particle moving through a magnetic field. The equivalent electric field in the rest frame of the H^- ion is

$$\varepsilon = 0.3\ \beta\gamma B \times 10^6 \text{ volts/cm} \tag{9}$$

where β and γ are as defined previously, and B is the magnetic field in kilogauss. The maximum electric field in the case of TRIUMF is about 2.0 MV/cm. Theoretical calculations of the lifetime of the H^- ion in this field have been made by Mullen,[5] Hiskes[12] and others, but they do not agree well with the experimental results of Stinson *et al.*[6] Using a function of the form

$$\tau(\varepsilon) = \frac{C}{\varepsilon} \exp\left(\frac{D}{\varepsilon}\right), \tag{10}$$

Stinson *et al.* found that $C = 7.96 \times 10^{-14}$ sec-MV/cm

and $D = 42.56$ MV/cm.

For $\varepsilon << D$, $\tau(\varepsilon)$ is a very rapidly decreasing function of ε. In our case, halving the magnetic field raises τ by a factor of 4×10^3. Hence eqn. (9) sets a limit on the maximum field. Letting the maximum hill field equal 5.76 kG will give a beam power loss of about 11.2% for TRIUMF.[4]

2.3 Magnetic Field Design

So far, for any given beam energy we can calculate γ, β, $\overline{B}$, and R. Two tasks remain. One is to find the hill width η which is consistent with B_{max} being less than 5.76 kG and $\overline{B}$ satisfying the isochronism condition. The other is to obtain the flutter and spiral angle necessary to satisfy the vertical focusing criterion. The techniques applied to solving these two tasks are inexact, as the relationship between the required field shape and the shape of the magnet pole piece is a complex geometrical function. An empirical solution has been applied using the approximate formulae discussed previously.

2.3.1 Hill Width

If the field were a square wave, we would have no problem calculating η, the hill width in degrees. That is, if the hill field and valley field were flat and equal to $\overline{B}_H$ and $\overline{B}_V$ respectively, then we can see from Figure 3 that, for an N-sector machine,

$$\frac{360}{N}\overline{B} = \eta\overline{B}_H + \left(\frac{360}{N} - \eta\right)\overline{B}_V$$

or

$$\eta = \frac{360\ (\overline{B} - \overline{B}_V)}{N\ (\overline{B}_H - \overline{B}_V)} . \qquad (11)$$

For TRIUMF, N = 6. The reasons are: 1) for $N \leqslant 4$, the beam will pass through the radial stop band resonances before it reaches 500 MeV;[10] 2) $N \geqslant 8$ will not yield enough flutter at large radii to permit adequate vertical focusing; and 3) N = 5 and N = 7 are inconvenient numbers to work with. Hence eqn. (11) becomes

$$\eta = \frac{60\ (\overline{B} - \overline{B}_V)}{\overline{B}_H - \overline{B}_V} . \qquad (12)$$

So if we know $\overline{B}$, $\overline{B}_H$, and $\overline{B}_V$, then η is determined. The average field $\overline{B}$ is fixed by the isochronism condition and we assume we can obtain any desired B_H by adding or removing steel to or from the return yoke. Hence the task is to find $\overline{B}_V$.

A real field looks more like the "rounded" curve in Figure 3. What is needed is some parameter which depends solely on the geometry of the pole tip and provides some measure of the "rounding" of the corners of the field. Such a parameter is the hill-to-hill distance D.[9] This is defined for a given radius R as the diameter of the largest circle that can be drawn centred on R and just touching the edges of the adjacent pole tips (see Figure 4). Figure 5 is a graph of D plotted against R for the Mk V-3 model magnet.

The problem of finding the hill width would be solved if we could find some way of relating the minimum valley field B_V, the average valley field $\overline{B}_V$, and the average hill field $\overline{B}_H$ to the maximum hill field B_H via some parameter which depends only on the geometry of the pole tip. D has proven to be very useful for this. The ratio

$$\xi \equiv \frac{B_V}{B_H} \tag{13}$$

is a good, single-valued function of D, as can be seen in Figure 6. Although D first increases and then decreases with radius, ξ remains single-valued in D to within ±5% for radii within 0 to 14.5 in. on the model. At the 15 in. radius, the dependence of ξ on D is not so good, as the abrupt cut-off of the pole tip at 15.5 in. begins to have an effect.

To a lesser extent, the ratio

$$\delta \equiv \frac{\overline{B}_V}{B_V} \tag{14}$$

is also single-valued in D. As shown in Figure 6, there is a definite difference between δ for increasing D and for decreasing D. Fitting a curve between the two results in a determination of δ to within ±3%.

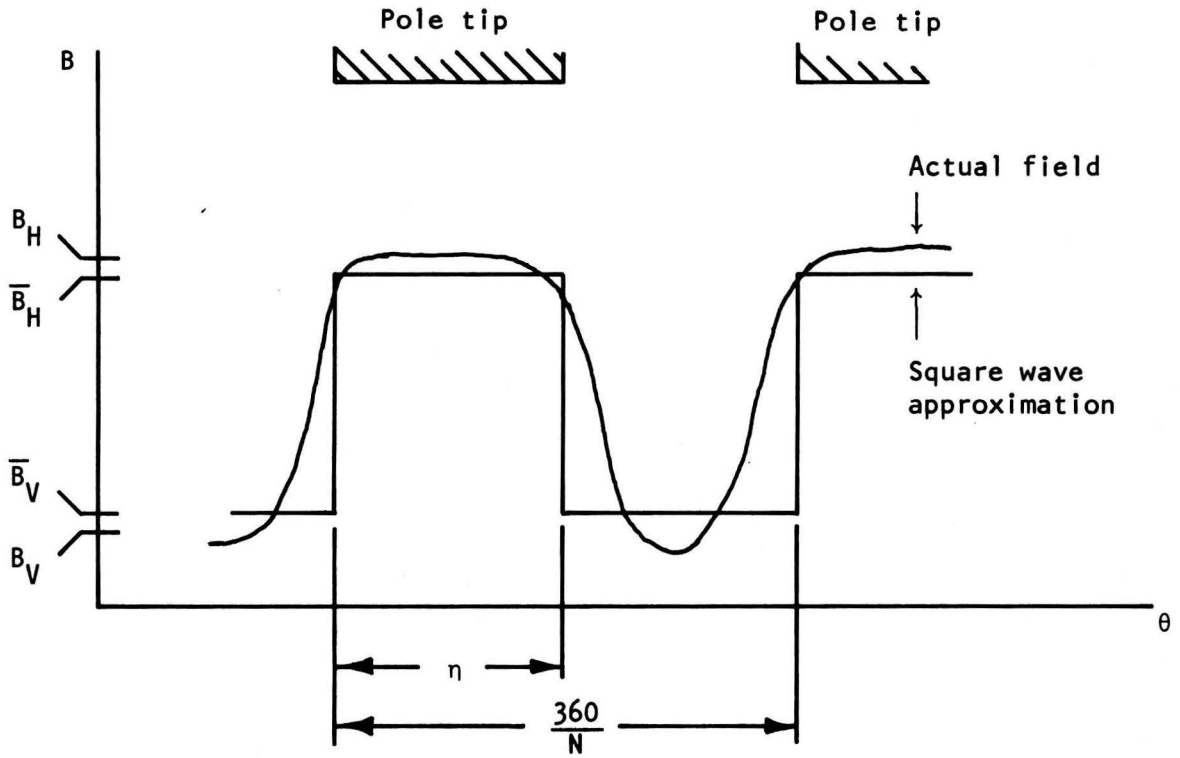

Figure 3. "Square wave" approximation to the azimuthal field contour

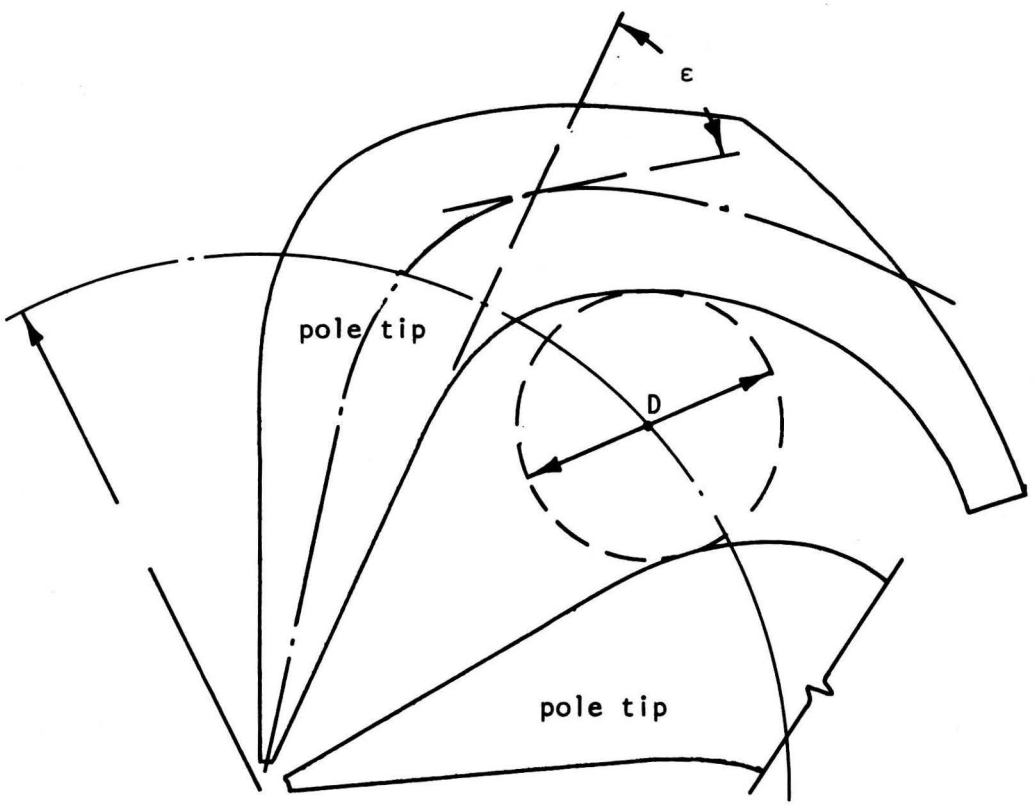

Figure 4.

Hill-to-hill distance and spiral angle of pole tip are defined

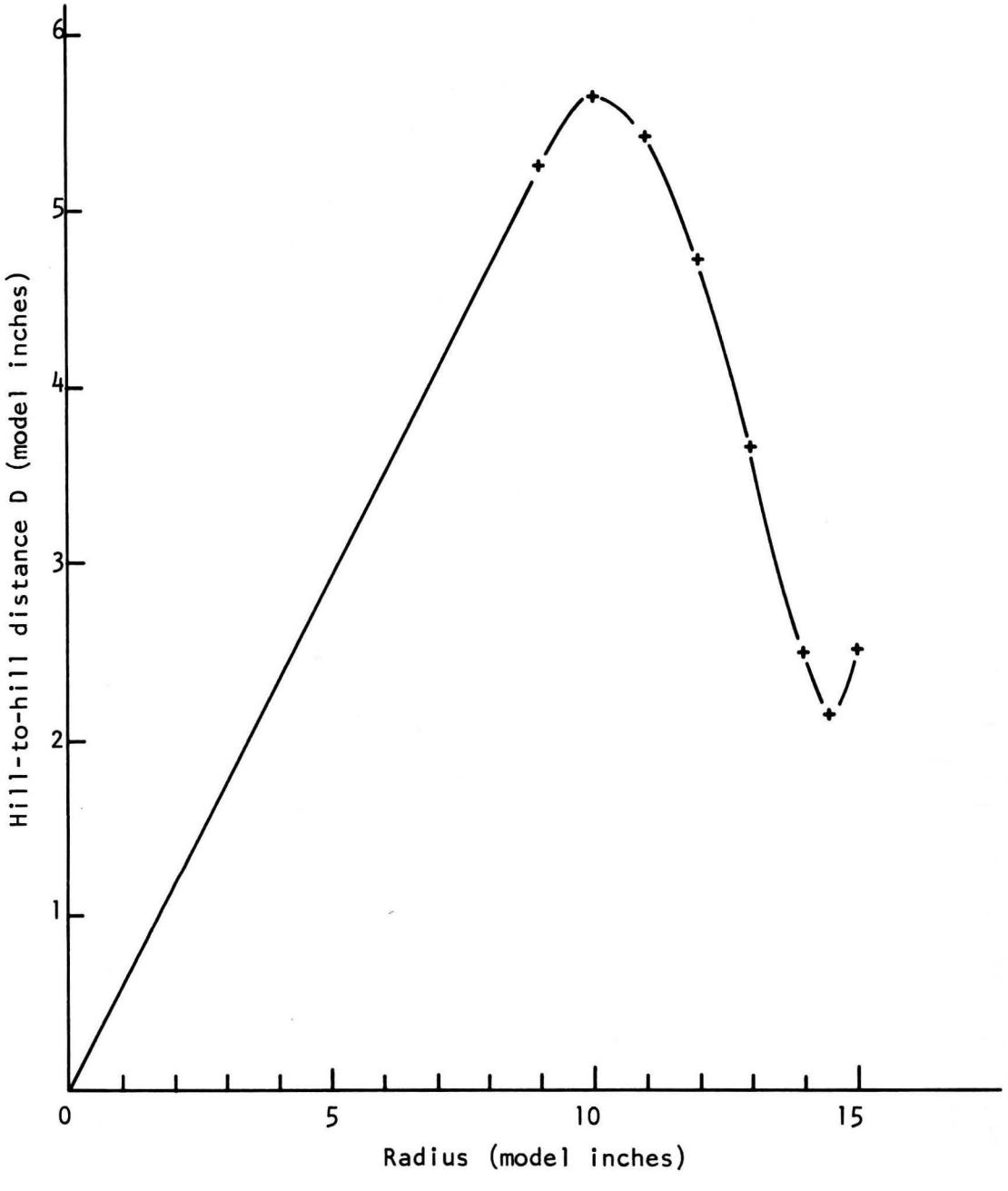

Figure 5. Hill-to-hill distance D plotted against radius for the Mk V-3 model magnet

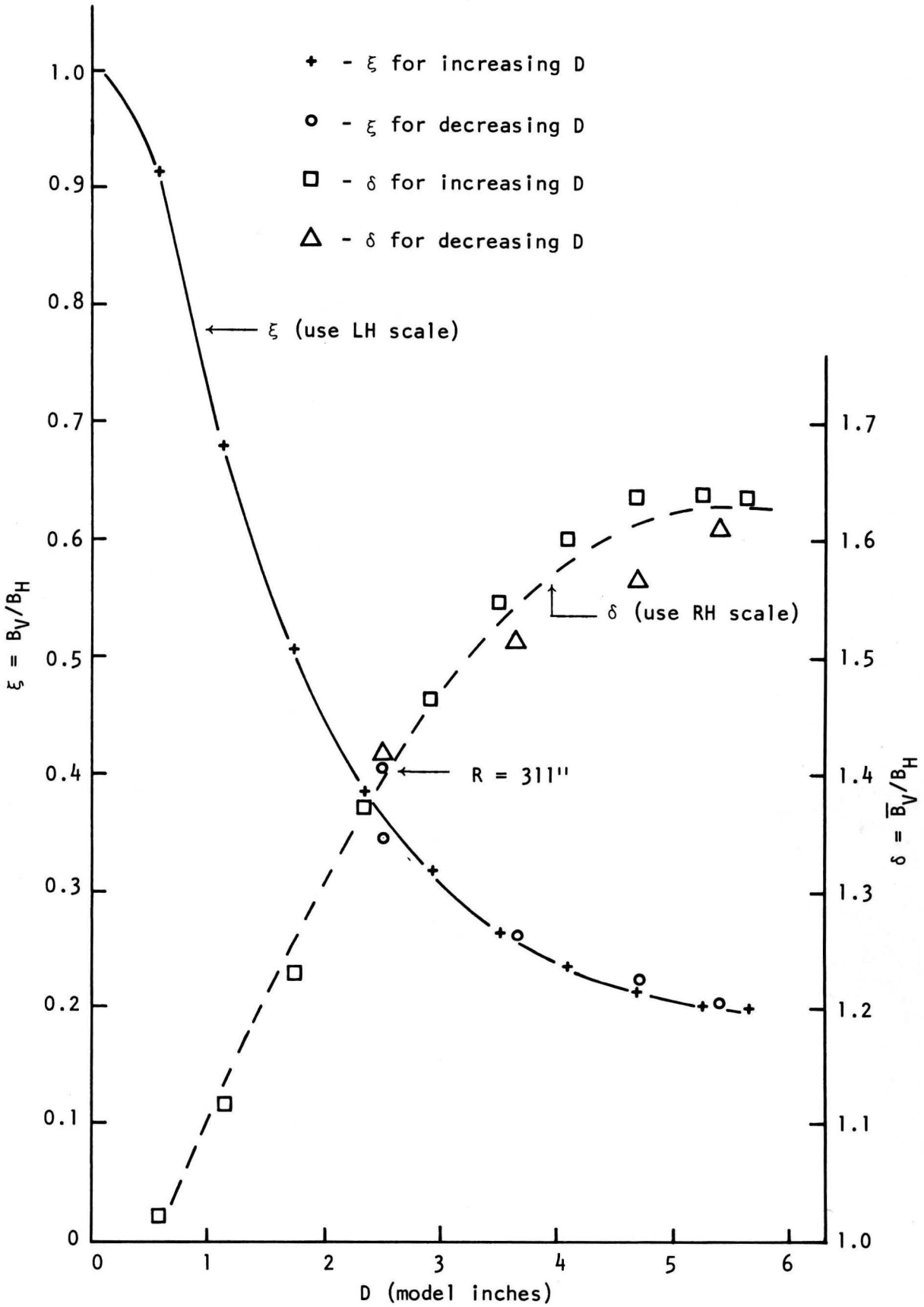

Figure 6. Parameters ξ and δ plotted against hill-to-hill distance for the Mk V-3 model magnet

The final parameter necessary to produce a square-wave field approximation is

$$\alpha \equiv \frac{\overline{B}_H}{B_H} . \tag{15}$$

We find that α is a function of the hill width in inches $R\eta'$ (see Figure 7), where η' is the hill width in radians. Three different processes are in evidence here. For $R\eta' << s$, where s is the gap length, α is a decreasing function of $R\eta'$, because the steel is effectively so far from the median plane that the field contour does not follow the steel contour. For $R\eta' > s$, α increases with $R\eta'$ because the field is now flat except near the edges of the steel. For large $R\eta'$, saturation in the steel causes the field to droop farther in from the edge, and hence α again decreases. In any case, since α varies over such a small range, it can easily be determined to within ±1%. It is not as critical a parameter as either ξ or δ.

By means of the parameters ξ, δ, and α, we are now able to produce a square-wave approximation to the real field, given just B_H and D. The necessary relations are:

$$\overline{B}_H = \alpha B_H$$

$$\overline{B}_V = \xi\delta B_H .$$

We can find η by substituting these values into eqn. (12) to get

$$\eta = \frac{60\ (\overline{B} - \xi\delta B_H)}{(\alpha - \xi\delta) B_H} . \tag{16}$$

B_H is an experimentally adjustable parameter. That is, we assume we can obtain any desired value just by removing or adding steel above the pole tip. The only restriction is that B_H must be less than 5.76 kG, because of the electric dissociation of the H^- ion. Hence, any reasonable-looking curve of B_H against radius can be used for designing a pole tip (some experience is required to determine what is a reasonable curve). The curve used in the Mk VI model magnet design is shown in Figure 8.

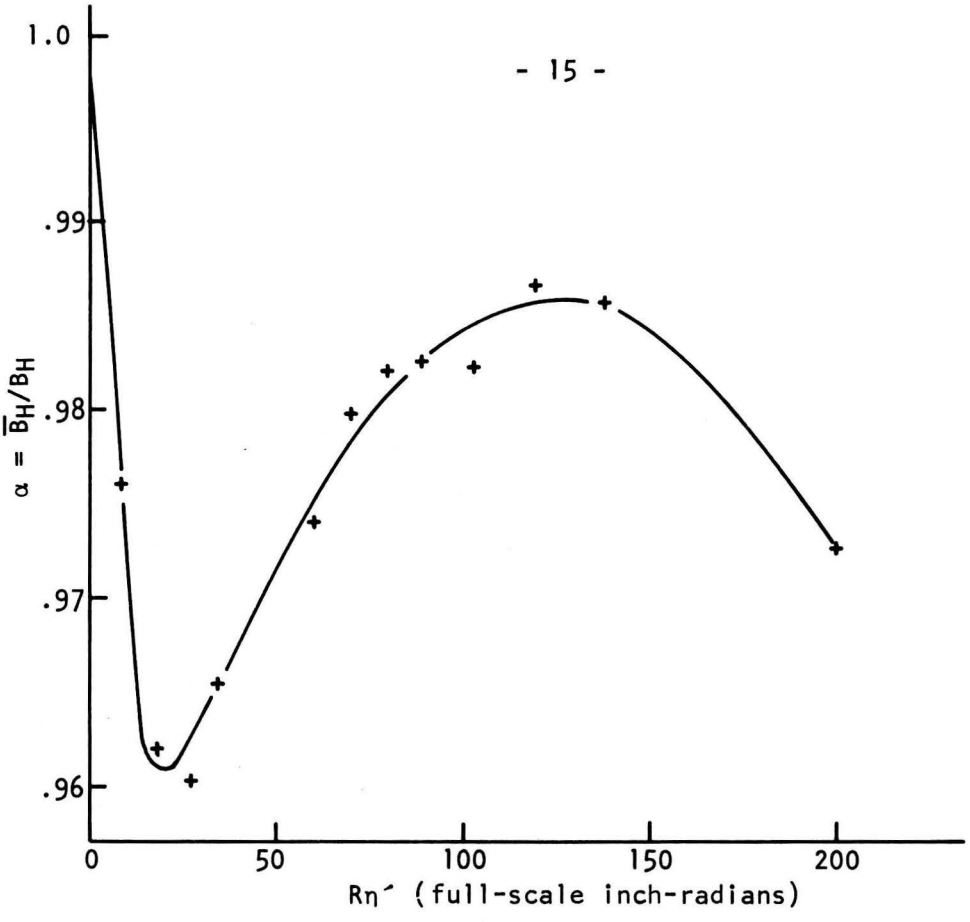

Figure 7. Parameter α plotted against Rη′ for the Mk V-1 model magnet

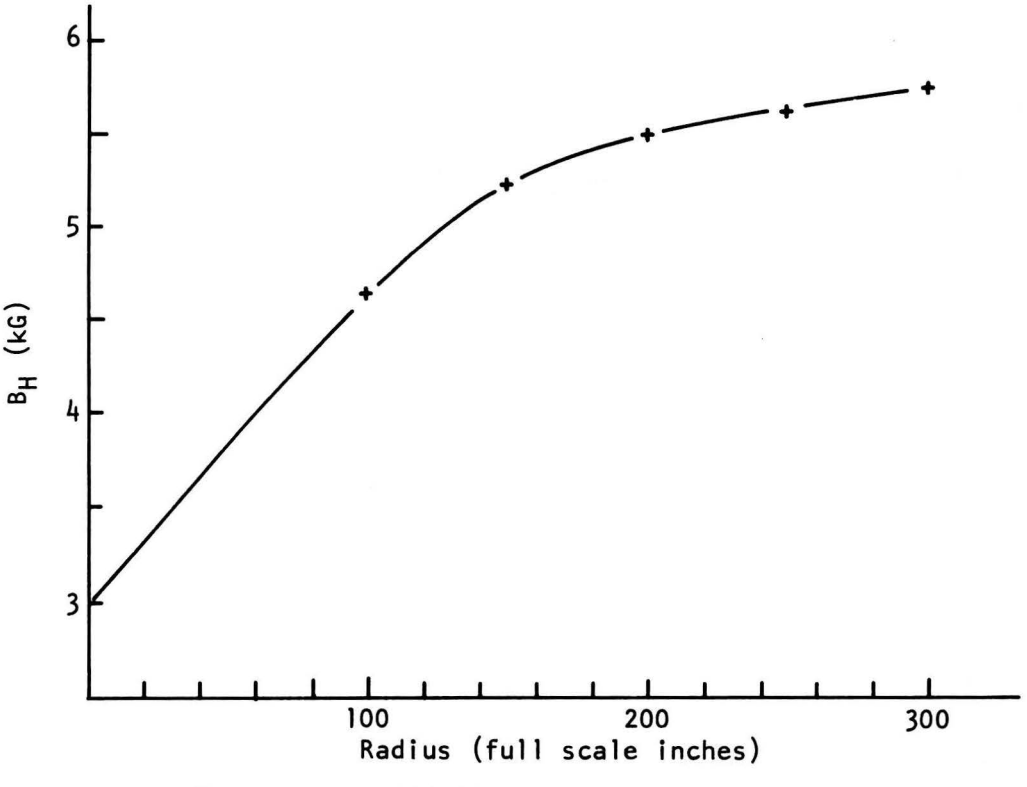

Figure 8. Maximum hill field as used in the design of the Mk VI magnet

2.3.2 Flutter

Once again, if the azimuthal field were square, computing the flutter would be trivial. However, it is not, and thus empirical techniques were used. Two methods were tried.

1) Fudge Factor

The fudge factor FF is defined as:

$$FF = \frac{\text{actual flutter}}{\text{flutter calculated for "square field}}. \qquad (17)$$

The flutter for a square field is

$$F^2 = \frac{(\bar{B}_H - \bar{B})^2\eta + (60 - \eta)(\bar{B} - \bar{B}_V)^2}{60\ \bar{B}^2}$$

$$= \frac{(\alpha B_H - \bar{B})^2\eta + (60 - \eta)(\bar{B} - \varepsilon\delta B_H)}{60\ \bar{B}^2}.$$

Some actual values of FF were obtained from the Mk III model magnet. An attempt was made to correlate them with some parameter of the magnet geometry. The best one seemed to be D, the hill-to-hill distance, but even that did not result in FF being single-valued, as can be seen in Figure 9. The solid line is a quadratic least-squares fit to the data points. An error of up to ±15% in the flutter can be expected by the use of this technique.

2) ϕD

It was found that the flutter is approximately a single-valued function of ϕD. ϕD is the product of D, the hill-to-hill distance, and ϕ, the valley width in radians. Figure 10 shows a plot of F vs ϕD, using data from two different models. The solid curve is a quadratic fitted via a least-squares technique to the Mk V-3 data points only. This curve gives values of F correct to within ±0.02, or ±15% at the largest radius, which is the most critical point.

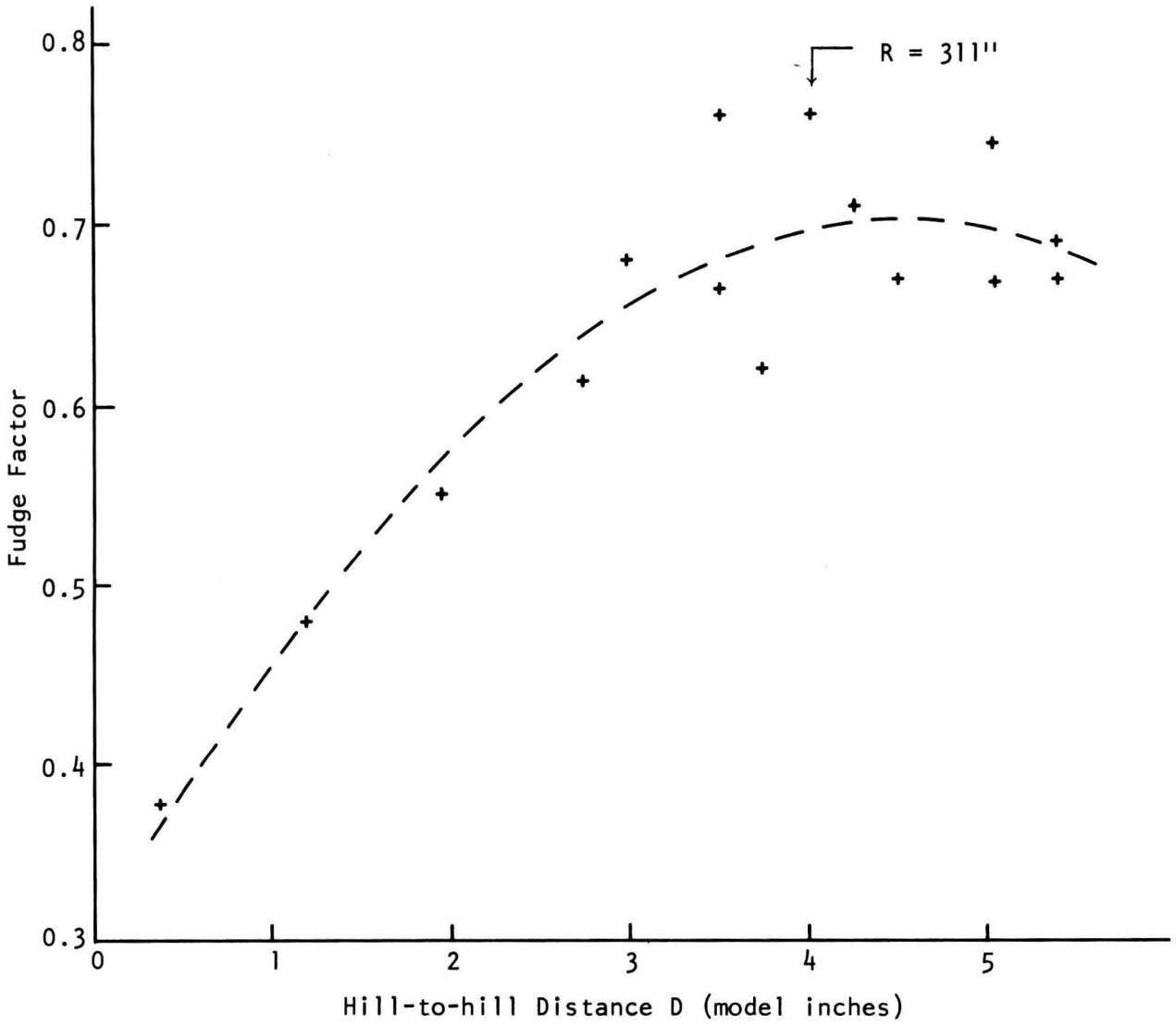

Figure 9. Fudge factor plotted against hill-to-hill distance for the Mk III model magnet. The dashed line is polynomial fit to the data points by a least squares technique.

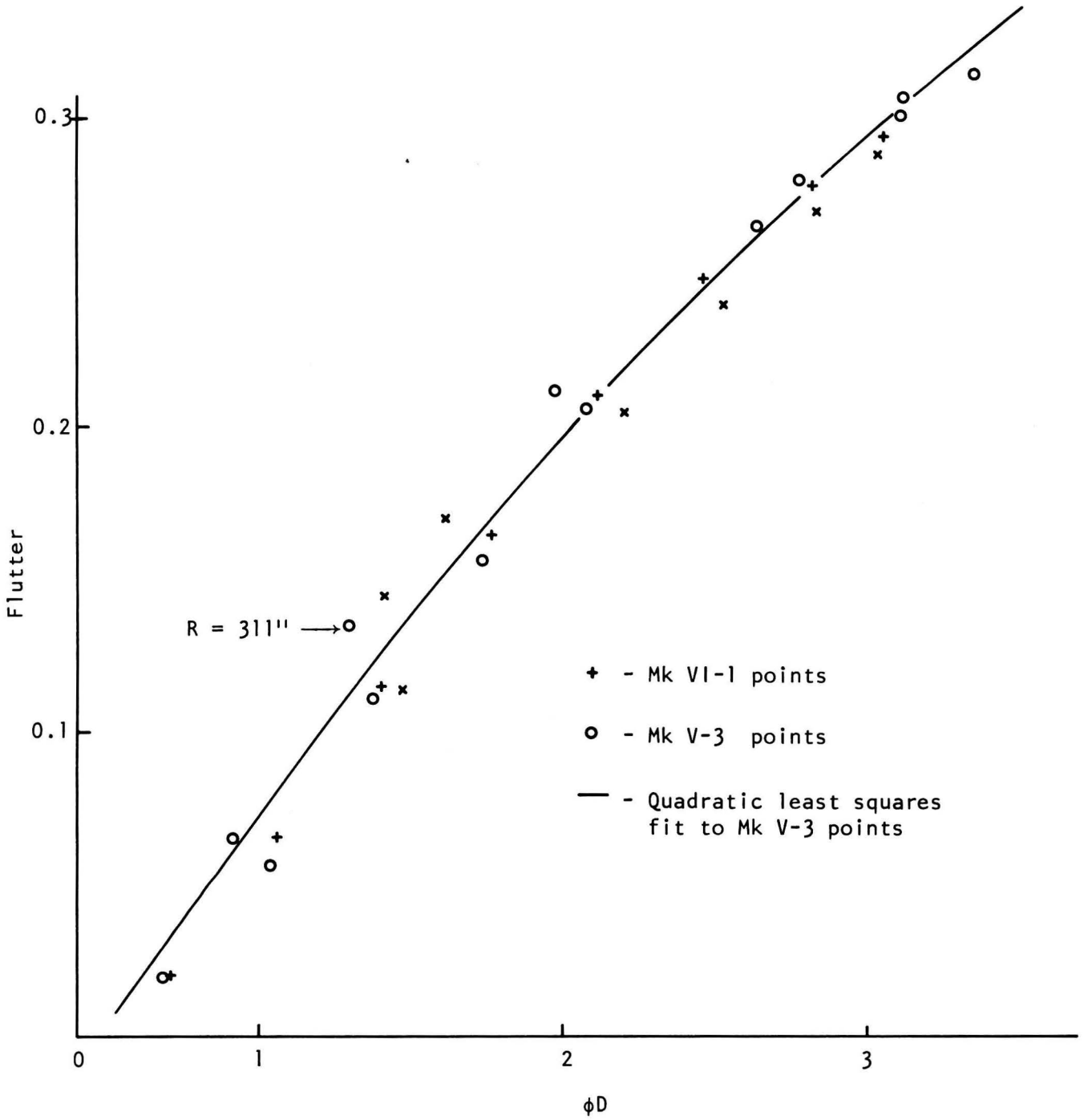

Figure 10. Flutter plotted against ϕD for the Mk VI-1 and Mk V-3 model magnets

The errors in either the fudge-factor or the ϕD method are roughly the same. The program to be described had an option whereby either technique could be used.

2.3.3 The Design Program

A computer program called "MAGNET", a listing of which can be found in Int. Rep. I-70-4 was written to assist in the design of a pole tip. It makes satisfactory predictions only for small changes in a pole tip. Its operation is as follows: The whole energy range of the machine is divided into many small increments. For each of these, γ, β, r, and $\overline{B}$ are calculated. Next, a curve of D vs R is assumed from the last magnet pole piece. From this and from the model measurements, values of ξ, δ, and α are found. Since we have assumed we can obtain any desired value of B_H, a curve of B_H vs R, which is similar to the last magnet, is used to obtain values of B_H and hence η for each energy increment. The techniques given in Section 2.3.2 are now employed to yield the flutter, and then by eqn. (8) we can calculate the spiral angle ε. The geometric relationship

$$h = \int_0^{\beta} \frac{\tan \varepsilon}{\beta} \, d\beta \qquad h = \text{hill angle} \qquad (18)$$

allows us to compute the actual angular positions of the edges of the pole tip to give the desired spiral angle ε.

Following this procedure through for all the energy intervals results in a pole tip. We can now iterate the whole process by measuring the hill-to-hill distance of this pole tip and putting it back into the program. When the hill-to-hill distance of the designed pole tip is similar to that used in the calculations, then the design is complete.

2.4 Mk VI Design

2.4.1 Results

It was decided to use the program to design the Mk VI pole tip. The Mk V pole tips had failed for various reasons. The Mk V-1 design, which had a hill width of 24.5 deg for $R \leqslant 150$ in., was unacceptable

because the high hill field required for isochronism at low radii was unattainable experimentally. The Mk V-3 pole piece had a central hill width of 26 deg, and although isochronism could be achieved, the pole tip was so wide that beam extraction became impossible. At large radii the pole tip overlapped the return yoke of the adjacent sector, resulting in a continuous vertical return yoke around the cyclotron. Also, the rather large hill width resulted in a low flutter, which gave rise to inadequate vertical focusing at low radii. On both the Mk V-1 and Mk V-3 models vertical focusing was sufficiently high for radii greater than 150 in.

On the basis of these two models, it was decided that the Mk VI design should have a central hill width of 25 deg. The general shape should be somewhere between the Mk V-1 and Mk V-3 designs, and hence most of the magnet parameters, such as ξ, δ, and F^2, should lie between those for the two Mk V models. At this point, the program was altered slightly. As mentioned in Sections 2.3.1 and 2.3.2, δ can be predicted to within $\pm 3\%$, and F^2 to within $\pm 15\%$. Since these parameters should lie between those found for the Mk V models, it was felt that more accurate values could be found by choosing some value between the Mk V-1 and Mk V-3 values for that particular radius. The formula used to find δ was

$$\delta = \left(\frac{\eta_0 - \eta_1}{\eta_3 - \eta_1}\right)\left(\delta_2 - \delta_1\right) + \delta_1$$

where $\eta_0 = 25$ deg, $\eta_1 = 24.5$ deg, $\eta_3 = 26$ deg, $\delta_1 =$ Mk V-1, $\delta_3 =$ Mk V-3. F^2 was found in a similar manner. It was hoped that this interpolation technique would reduce the error in δ to $\pm 1\%$, and F^2 to less than $\pm 5\%$.

A pole tip was built using this design. The results are shown in Figures 11 and 12. Isochronism was excellent; the maximum difference was 75 G. Figure 11 shows the difference between the isochronous field and the actual average field which has been normalized to the design hill field. The normalization was necessary because the steel return yoke was not the correct shape required to obtain the design B_H.

Unfortunately, ν_z was inadequate (see Figure 12). The design ν_z was 0.35, but the actual ν_z reached 0.25 at only one radius. The reason for this discrepancy is immediately apparent if we plot F^2 vs E, as in

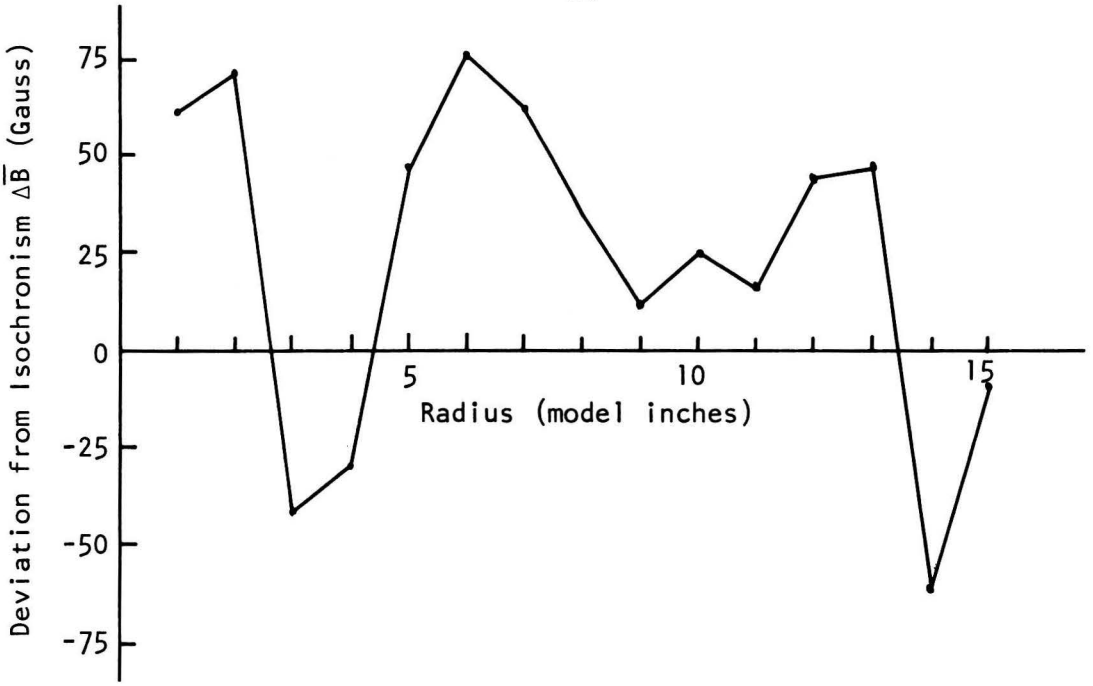

Figure 11. Deviation from isochronism for the Mk VI-1 Mod 0 model magnet.

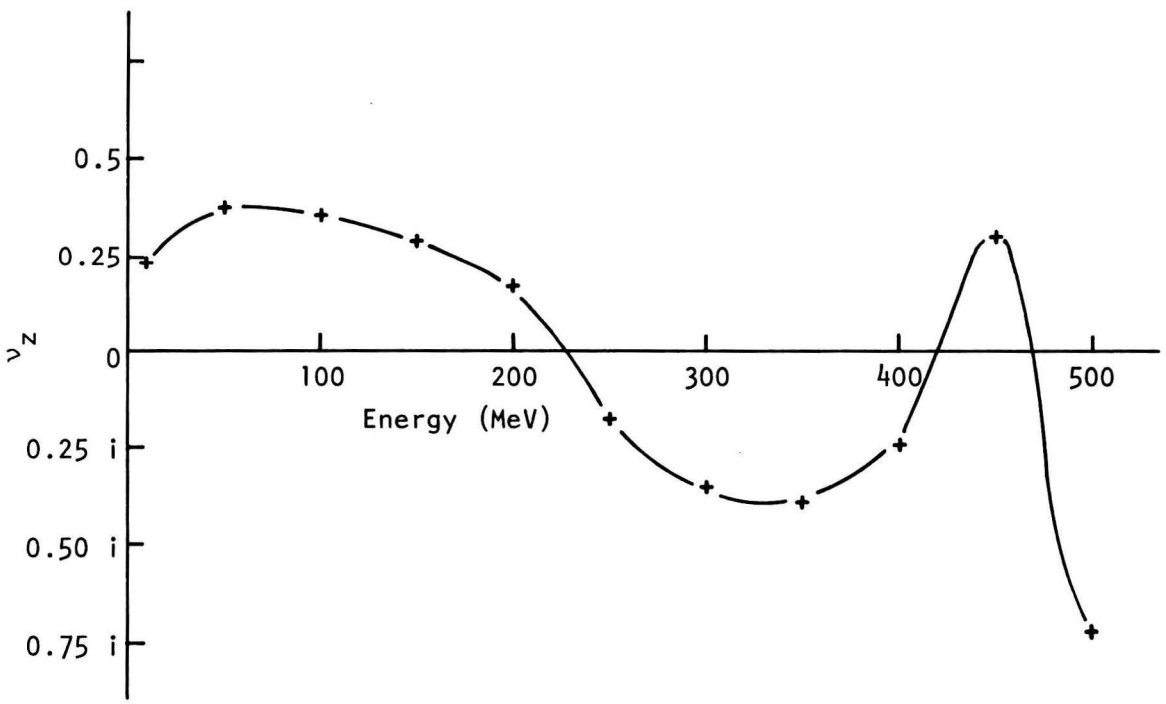

Figure 12. Vertical betatron frequency ν_z plotted against energy for the Mk VI-1 Mod 0 model magnet. Imaginary values of ν_z imply that the beam is not stable and will blow up in the vertical direction.

Figure 13. The program badly overestimated the flutter, and hence it did not allow enough spiral angle to maintain ν_z. At 500 MeV, the error in flutter $\Delta F^2 = 0.024$. By the use of eqn.(8), we find that the error in ν_z caused by ΔF^2 is

$$\Delta(\nu_z^2) = \Delta F^2(1 + 2 \tan^2\varepsilon)$$
$$= 0.24.$$

There is also a small contribution to $\Delta\nu_z^2$ arising from the inability of the field to follow the pole tip shape. This appears as an error in the spiral angle. Figure 14 shows the design spiral angle of the pole tip plotted against energy, and the actual spiral angle of the magnetic field, as computed from the phase of the 6th harmonic. The two curves agree well except around R = 260 to 290 in. This discrepancy is due to the positioning of the return yoke steel above the valley (see Figure 1), causing the field to lag. At the worst point (R = 280 in.), $\Delta\varepsilon = 5$ deg, which corresponds to a change in ν_z^2 of

$$\Delta\nu_z^2 = 4F^2 \tan\varepsilon \sec^2\varepsilon \, \Delta\varepsilon$$
$$= 0.16.$$

However, $\Delta\varepsilon$ then decreases, and at 500 MeV $\Delta\varepsilon = 1$ deg, which corresponds to

$$\Delta\nu_z^2 = 0.10.$$

While this effect is annoying, it is not catastrophic, and can easily be corrected for by the use of shims. However, the error in flutter is more serious, as it cannot be shimmed out without ruining isochronism.

The reasons for the large ΔF^2 are not hard to see in hindsight. The two curves of F^2 vs R used in predicting the flutter were taken from two models, neither of which actually had an isochronous average field. If they had, their hill widths would have been different, resulting in different flutter curves. Another, probably more important, reason is the zero error in the spiral angle, which will be explained in the next section.

Although ν_z was quite bad, this pole tip was sufficiently good that it could be modified to obtain a pole tip which focused and was isochronous out to 500 MeV. Another Mk VI design was done at the same time, but

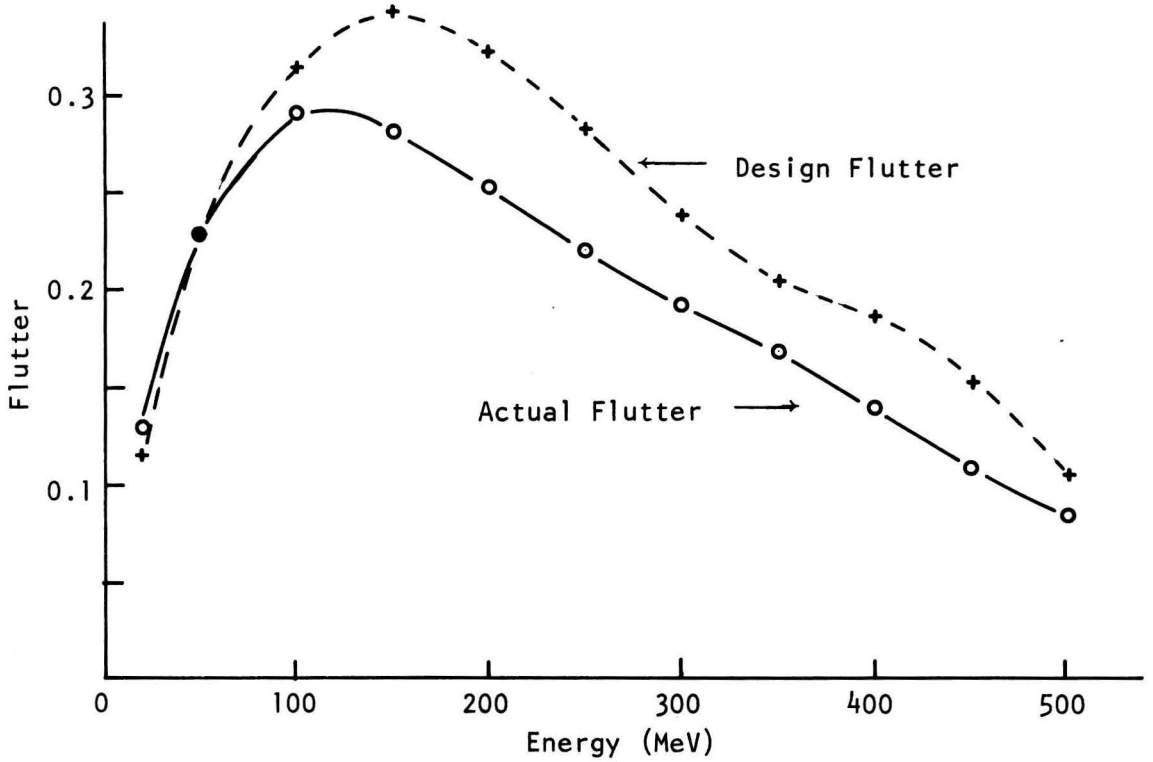

Figure 13. Design Flutter compared to Actual Flutter for the Mk VI-1 Mod 0 model magnet

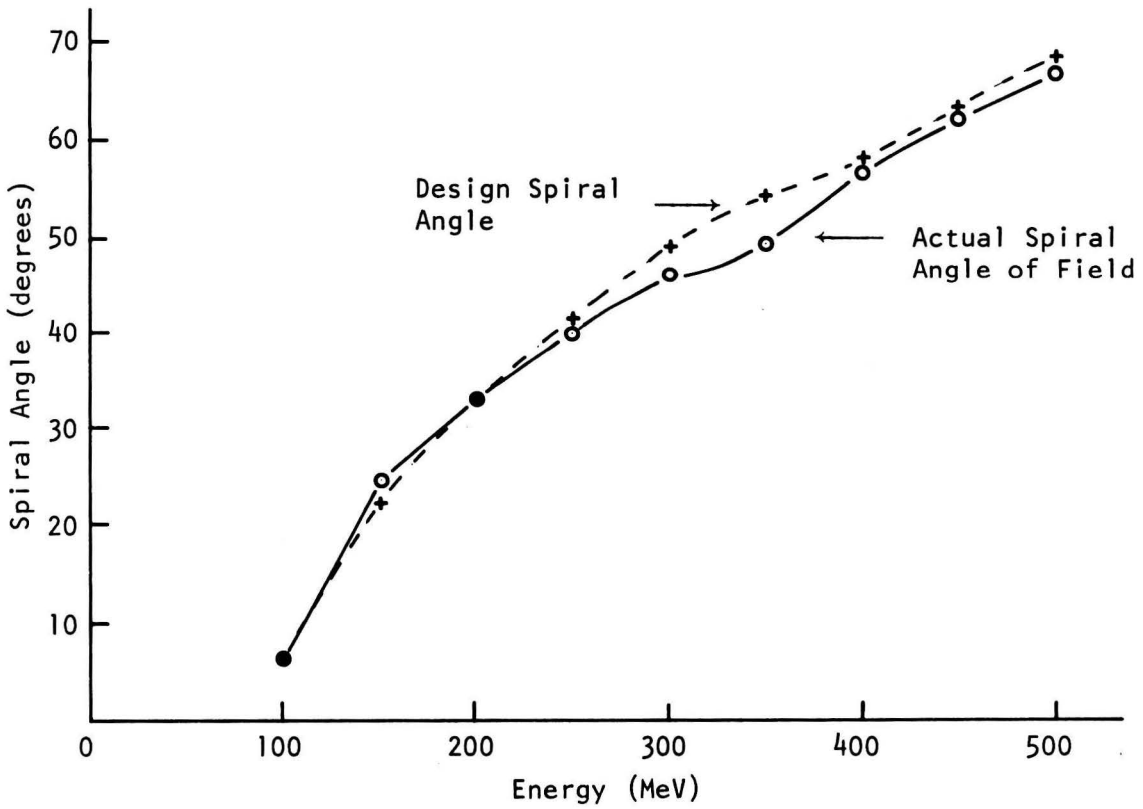

Figure 14. Design Spiral Angle compared to the Actual Spiral Angle for the Mk VI-1 Mod 0 model magnet

without the use of this program. It proved to be unsatisfactory because of isochronism problems. Hence it is felt that the program, even in this state, served a useful purpose in the design of the magnet.

2.4.2 Zero-offset in ε

Once it was discovered that the flutter had been predicted badly by the interpolation technique, the program was rerun using the ϕD technique described in Section 2.3.2. This produced a pole tip with a very large spiral. Extraction would be impossible with this magnet without drilling holes in the return yoke.

At this point, the program was again modified. A zero-offset spiral angle was included in the formula for ν_z^2 (eqn. 8). The reason for this can be seen in Figure 2. For $R \leqslant 150$ in., the actual spiral angle of the field was zero, but use of eqn.(8) gave a spiral angle of about 14 deg. Clearly, the assumption made earlier, that this error at low radii did not matter, was wrong. The hill angle h is effectively the integral of the spiral angle and is hence a cumulative parameter. Even though the spiral angle is wrong by only a little bit, its total effect on h is quite large. The modified form chosen for eqn.(8) is

$$\nu_z^2 = -\beta^2\gamma^2 + F^2[1 + 2(\tan^2\varepsilon + \tan^2\varepsilon_0)] \qquad (19)$$

where $\varepsilon_0 = 14$ deg. In this form, ε_0 has a large effect at low ε, but a negligible effect at large ε. That this does indeed approximate the full ν_z^2 expression somewhat better can be seen in Figure 15. Curve 2 is the actual spiral angle of the field, curve 1 is calculated using eqn.(8), and curve 3 uses eqn.(19). The spiral angle is still overestimated by about 2 deg for 200 in. $\leqslant R \leqslant$ 250 in., and underestimated by the same amount around R = 305 in. However, this is approaching the limits of our experimental accuracy in determining ε, and is certainly much better than the 14 deg error previously for $R \leqslant 150$ in.

At the time of writing this report, a working pole tip design had been achieved. It is basically the Mk VI-1 design as described in the previous section, but with several modifications. Called the Mk VI-1 Mod 9 design, it is isochronous to within ±100 G, and focusing is good; $\nu_z = 0.3 \pm 0.1$ except at R = 305 in., where $\nu_z = 0.65$. Hence we have a

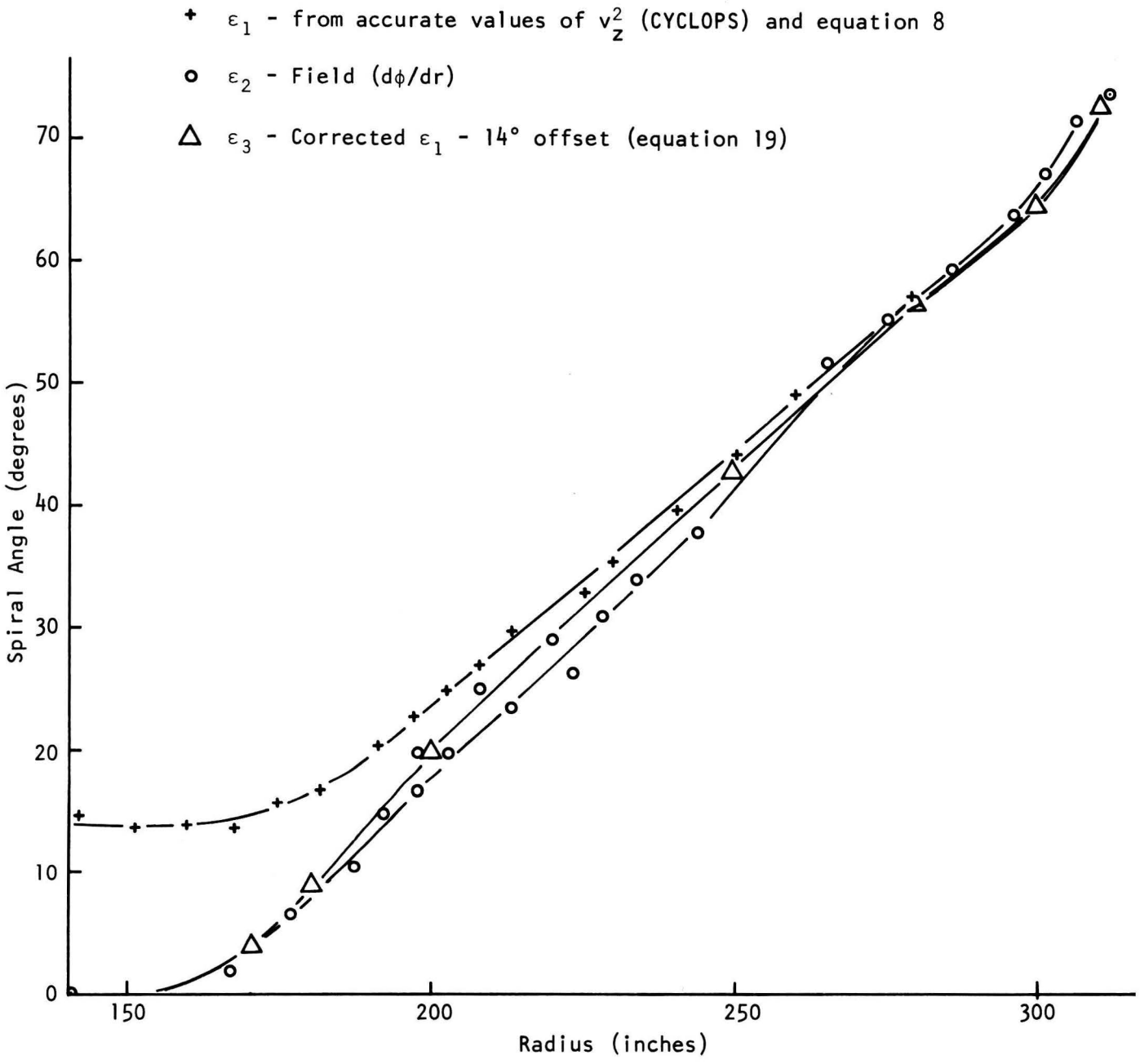

Figure 15. Spiral angle predictions from equations 8 and 19 compared to the actual spiral angle of the field

pole tip which works, and we can check the results of program MAGNET by comparing them to this design.

The program was modified to use eqn.(19) rather than eqn.(8). A run using the same input data as used for the Mk VI-1 design produced a pole tip fairly similar to the Mk VI-1 Mod 10 pole tip. (The Mk VI-1 Mod 10 pole tip is very similar to the Mod 9 tip. It was used because data on it were more readily available.) Figures 16 and 17 show the comparison. The spiral angles are within ±5 deg of each other. Although the Mod 10 pole tip seems to have a non-smooth spiral angle curve, most of the bumps will not appear in the field, as the field contour will not follow irregularities in the steel smaller than the gap width of 20 in. Hence the smoother pole tip predicted by the program should produce the same spiral angle in the field as the Mod 10 pole tip. The hill angles are within ±1 deg of each other, which is also encouraging.

The hill width of the calculated magnet is much higher than that for the Mk VI-1 Mod 10 pole tip. The reason is that this is not a finished design - i.e., the curve of D vs R has not been iterated. The hill width η is very strongly dependent on D. D in turn is strongly dependent on the amount and shape of the steel beyond 312 in., which is not set by the program. Hence considerable work and a certain amount of judgement must be used when iterating D. On each iteration, the program sets the new hill-to-hill distance out to R $\approx$ 280 in., but for larger radii the programmer must choose an appropriate and physically-realizable D. Two or three iterations are usually sufficient. In the calculation above, only one iteration was performed, using the hill-to-hill distance of the Mk V-3 model magnet.

It is not to be expected that the program will generate a perfect pole tip. As can be seen in Figures 6, 9 and 10, the parameters ξ and F both depart from being single-valued functions of the magnet geometry as the radius approaches the "corner" of the pole tip. The situation at this radius is very critical, as regards beam extraction. The main criterion for ease of extraction is $\eta + h \lesssim 60$ deg. Otherwise, the pole tip will bend over into the return yoke for the adjacent pole tip. For the Mk VI-1 Mod 10 magnet, $\eta + h = 61$ deg, and η must still be increased to correct for isochronism. Hence the point at which the program becomes least accurate is also the point where the design is most critical. A model must be used to check the design.

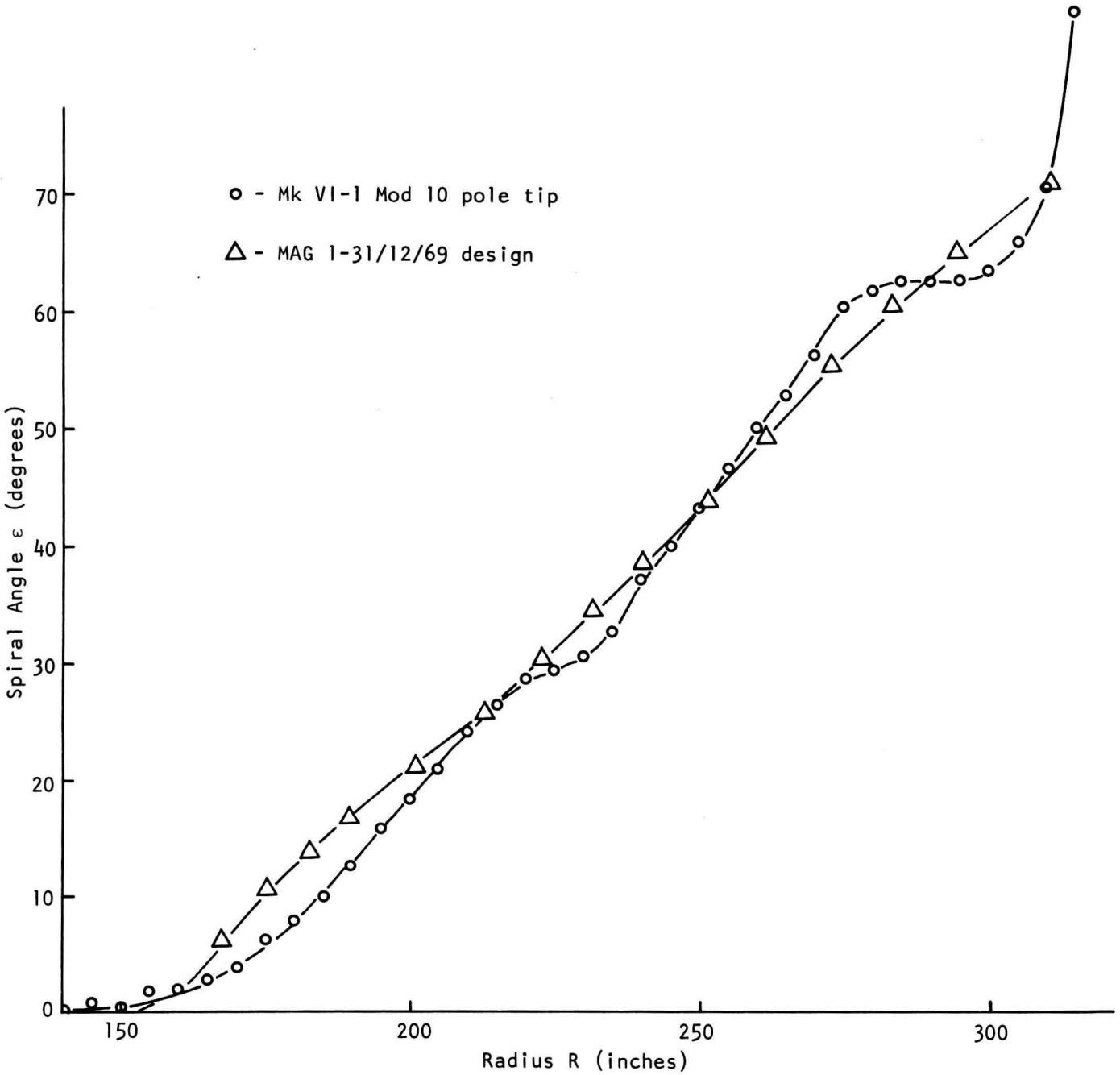

Figure 16. Design spiral angle plotted against actual spiral angle for the Mk VI-1 Mod 10 model magnet

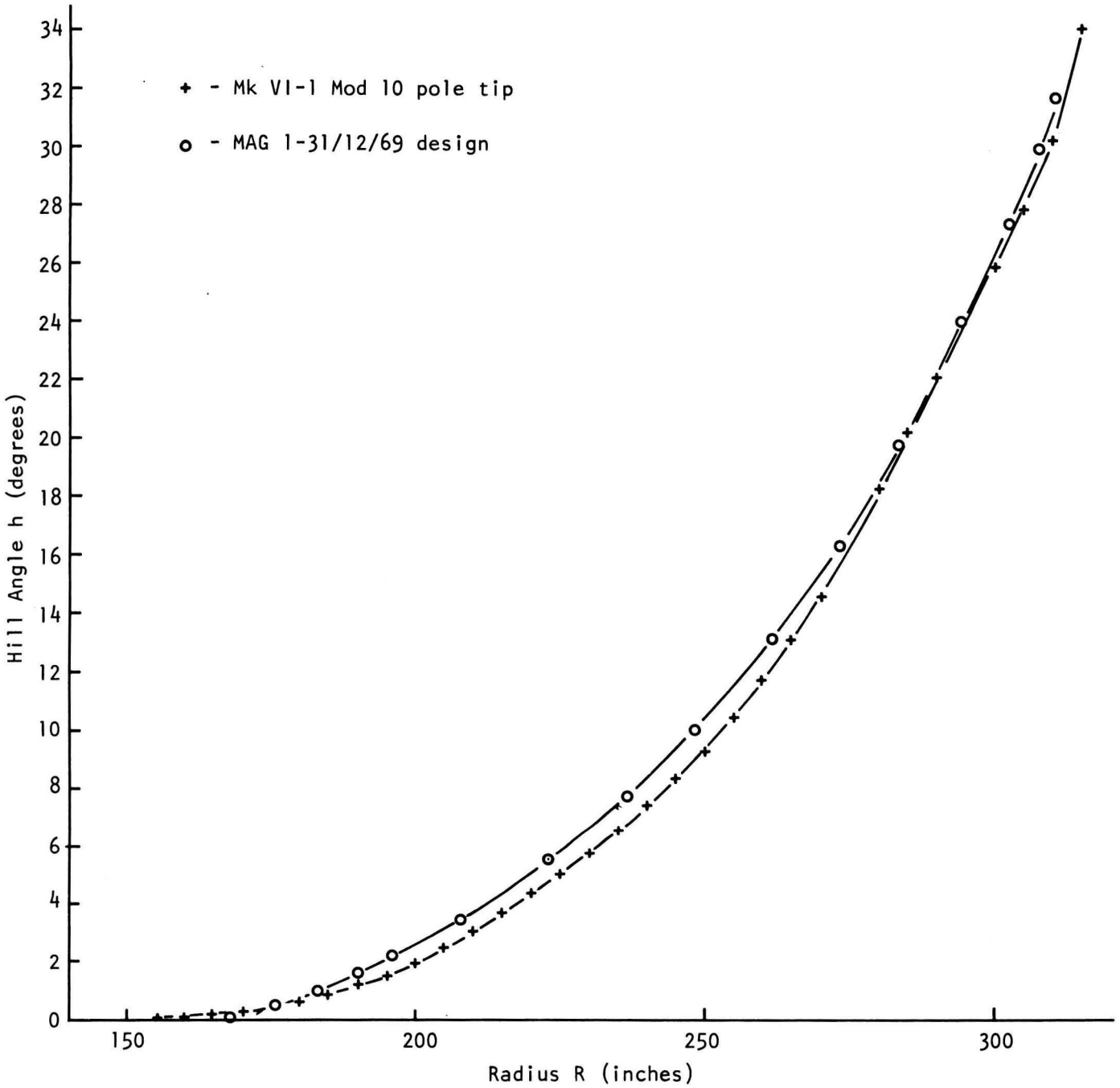

Figure 17. Hill angle h of the design and actual pole tips for the Mk VI-1 Mod 10 model magnet

3. AZIMUTHAL MAGNETIC FIELD PREDICTION

3.1 Introduction

The problem of finding the magnetic field strength inside a complex magnet structure when high fields are involved has not been solved. The reason is that the permeability of the steel is a function of the field. This is in contrast to the electric field problem, where the dielectric constant is in general not dependent on the field strength, and hence Maxwell's equations can be solved. In this section, other less general techniques for finding the field will be investigated.

3.2 Fits to Various Formulae

An attempt was made to fit the azimuthal field contours with various analytical expressions, and then relate the expressions to the magnet geometry. The first fit that was tried was of the form $B = a\theta^n$ where B is the field and θ is the azimuthal angle. The valley field only was fit by this formula, and the hill field was assumed to be flat. A good fit was obtained for $4 \text{ in.} \leq R \leq 10 \text{ in.}$, but for large radii, the spiral angle caused an asymmetric valley field which could not be fit by our symmetric formula, and for small radii, the assumption that the hill field was flat did not hold. Also, no useful correlation could be found between the parameters a and n and the magnet geometry.

A Saxon-Woods expression was also tried:

$$B = B_0 - \frac{B_0}{1 + e^{(\theta-\theta_0)/a}} .$$

The advantage of this formula is that it does have the right sort of curve. For our field contours, two independently-varied Saxon-Woods curves were added together. Figure 18 shows a least-squares fit to a typical field curve taken from the model magnet. Curves II and III are the two curves, and curve IV is their sum. The fit is quite bad, especially at the "corners", where the error is ±500 G. No attempt was made to correlate the parameters to the magnet geometry.

Other types of fits were tried, but they were even less successful.

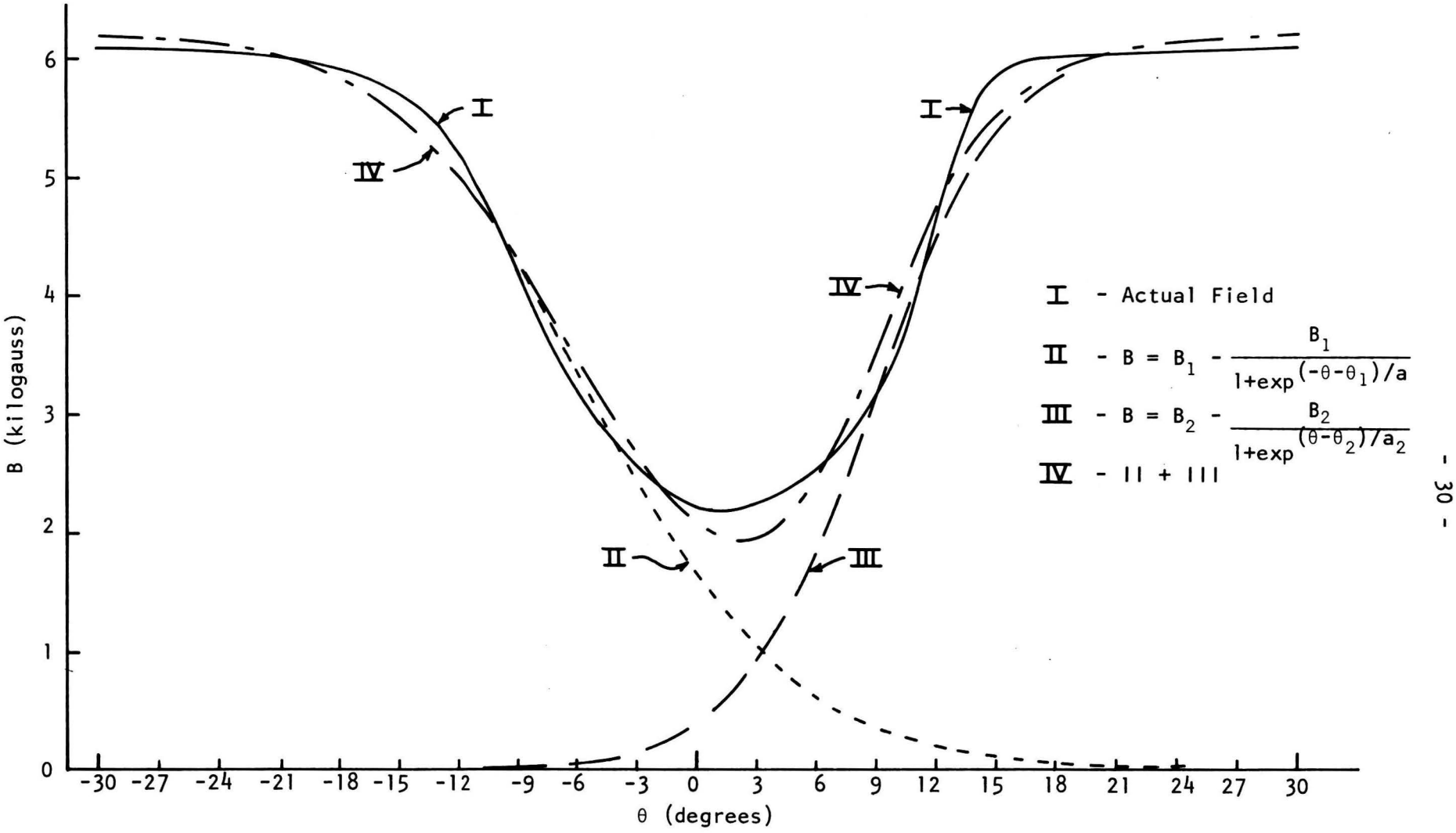

Figure 18. Saxon-Woods Approximation to Field Curve

3.3 Experimental Field Curves

An experiment was performed to see how the field varies with distance from the pole tip. Figure 19 shows the experimental arrangement. Two steel plates were attached to the poles of a Varian V-4000 electromagnet. The gap was set to 1.000 ± 0.001 in. The steel was the same as that in the model magnet pole tips, both in composition and in thickness. It was hoped that the field along the median plane both inside and outside the gap would closely resemble the field produced by the model magnet. Readings were taken with a Hall probe, using the edge of the steel as the zero point (i.e. $D' = 0$). Three sets of pole tips were used, the radii of curvature of the relevant edges being 5.5 in. concave, 5.5 in. convex, and infinity (a straight edge). These curvatures are roughly those encountered in the model magnet. Three runs were taken for each set of pole tips, with the maximum field set at about 3, 6 and 10 kG. For each set-up, D' was varied from -1.5 in. to +4.0 in. The fields obtained are plotted in Figure 20 (a,b,c).

A computer program was then written to generate field contours of a real pole tip using this experimental data. The field at any point is computed by calculating the perpendicular distances to the nearest edges of the two closest pole tips, looking up in Figure 20 the field contribution from each pole tip, and adding the two together. By following this procedure for many points along a radius, one can obtain an azimuthal field contour. In this case, for ease of programming just one of the B vs D curves in Figure 20 was used - the 6 kG, $R = \infty$ curve. The differences between this curve and any of the others are just second-order effects, and we can at least find out how well the method works by using only one curve. The field contours obtained so far are now multiplied by the ratio of the maximum hill field of the real magnet, to the maximum field of our calculated contour. This is an acceptable procedure, as we can obtain virtually any desired hill field by adding or removing steel above the pole tip.

The first results were not encouraging. Although the general shapes of the field contours were produced, the valley field was too high. The reason is that the close proximity of the coils and the supporting

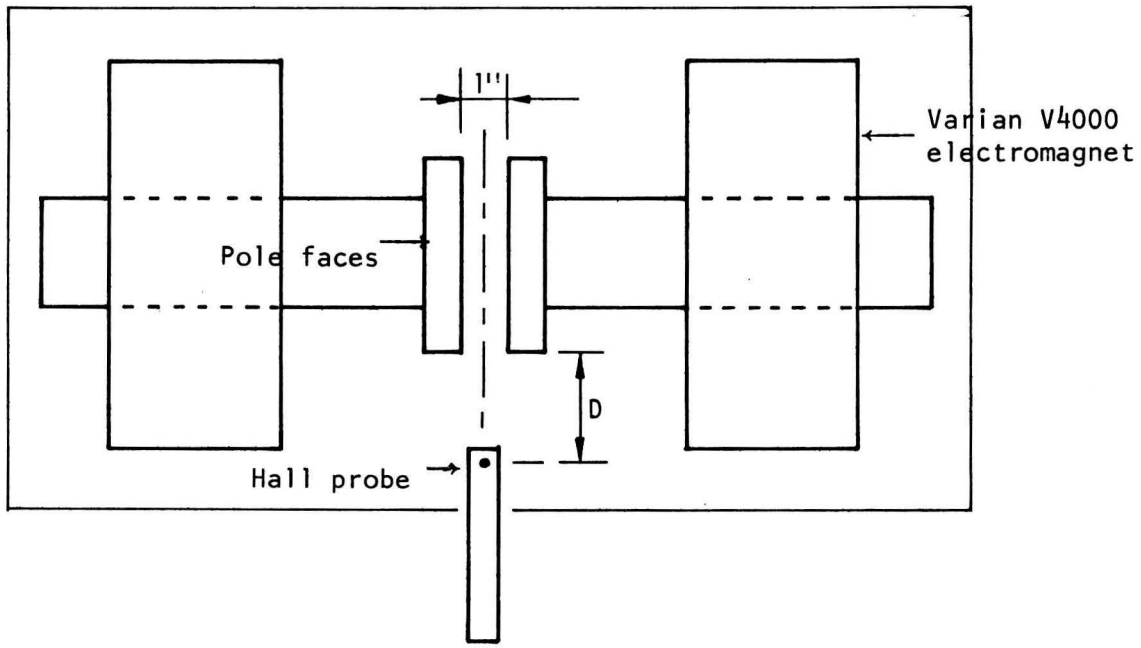

Pole Faces:

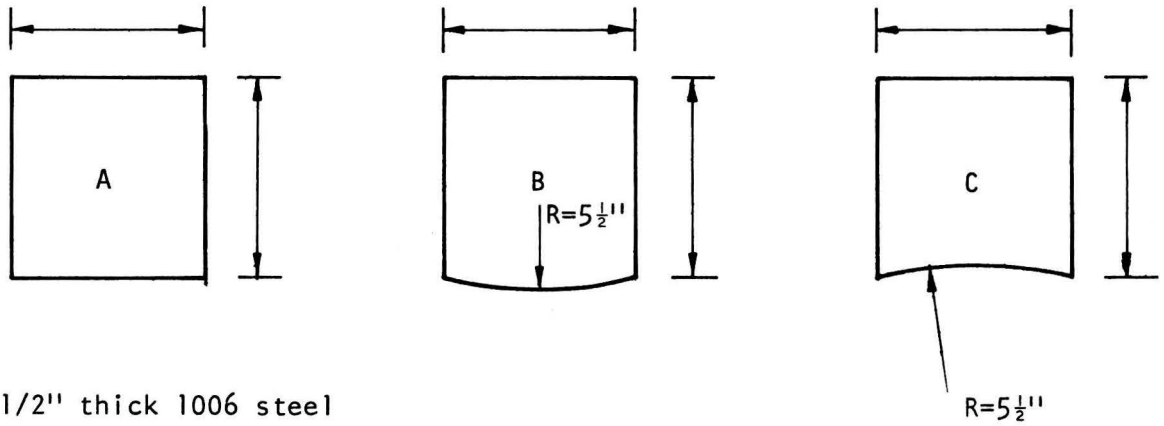

1/2" thick 1006 steel

Figure 19. Experimental arrangement to determine variation of field with distance D

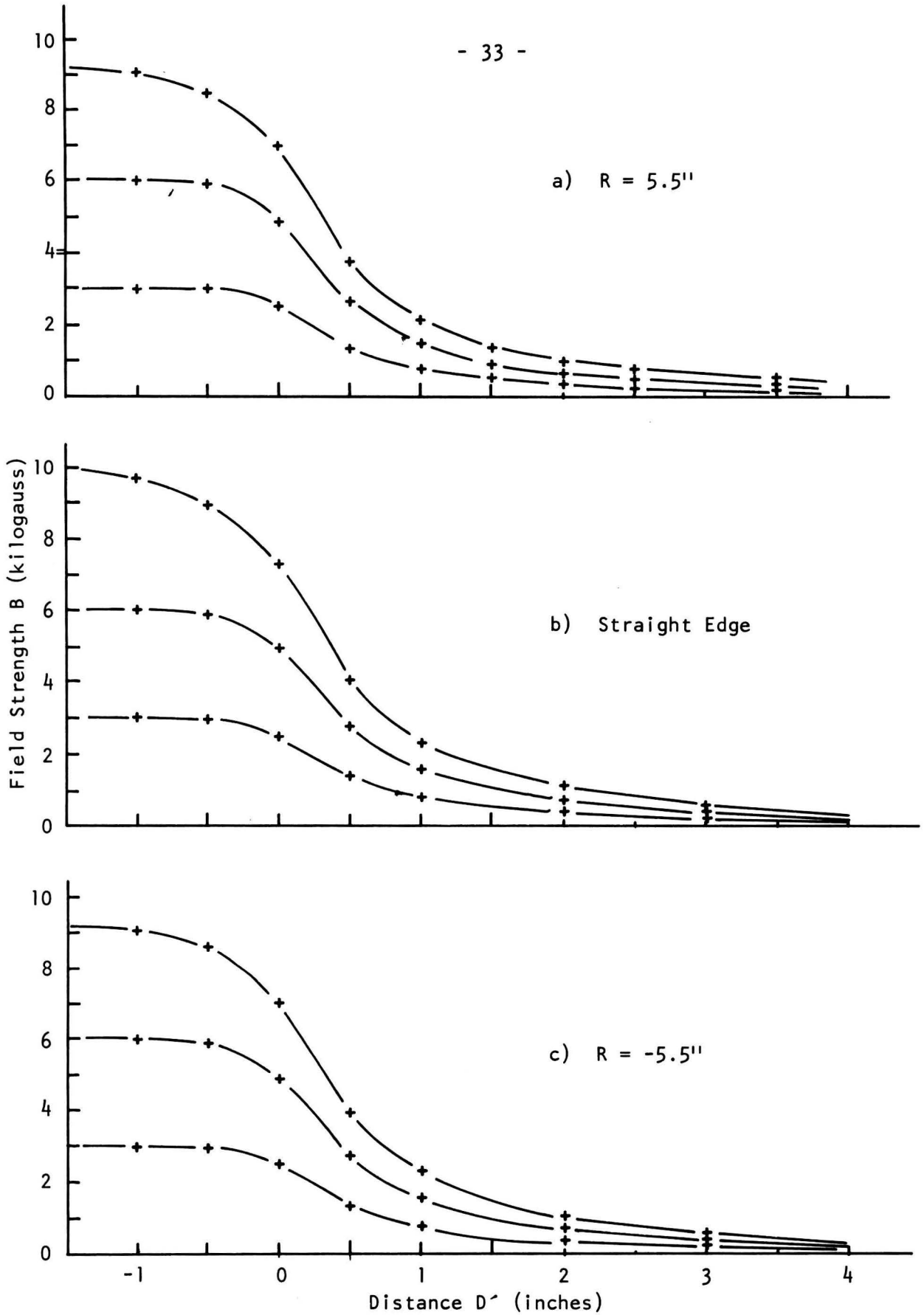

Figure 20. Field variation with distance for the experimental arrangement of Figure 19. R refers to the radius of curvature of the pole tip being used.

structure in the Varian electromagnet causes the fringing field around it to be higher than that around a pole tip. This problem was overcome by the following technique. We know what the minimum field should be for a given pole tip from the parameter ξ (see Section 2.3.1). The generated field contours can now be expanded to get $B_H - B_V$ correct, and shifted until the average field is correct.

The modified program was run using the accurately measured data points for the Mk VI-1 Mod 10 pole tip. The listing of this program is given in Int. Rep. I-70-4. Results were quite good. Table I compares the flutter and average field of the generated contour with that of the field actually obtained from this pole tip. Neglecting radii 14 in. or greater, the maximum error in $\overline{B}$ was 66 G, or 2%, and the maximum error in flutter is 7.9% at R = 2 in. The two radii with the greatest error in $\overline{B}$ are plotted in Figure 21. In the 4 in. radius curve, the minimum valley field has been incorrectly predicted; that is, ξ is wrong by about 3%. In the 12 in. radius curves, we see that the hill field of the actual model magnet is not flat. Thus, in a sense, the real field is not correct, since the field could have been made flat by changing the return yoke steel. The program will generate a field with a nearly flat hill. Even though we have these two error sources, we have still predicted $\overline{B}$ within ±70 G, and F^2 within ±6% in the range 3 in. $\leq$ R $\leq$ 13 in.

As with the magnet program, this program does not work well for very small or large radii. For small radii, the width of the pole tip is becoming less than the gap size, and hence the contour of the field will not conform to the geometry of the pole piece. At large radii, the "corner" in the steel where the spiral has been abruptly cut off has an effect. Obviously the field a distance away from a "corner" will not be the same as the field the same distance from a straight edge. A two-dimensional grid of points would have to be measured around an appropriate pole face, and then the program would have to be modified to mesh these points smoothly with the field contours obtained over other parts of the pole tip. The problem was not attempted.

TABLE I

COMPARISON OF PREDICTED B AND F WITH ACTUAL
B AND F FOR THE MK VI-1 MOD 10 MODEL MAGNET

R (model in.)	Actual Mk VI-1 Mod 10					
	$\overline{B}$ (kG)	F^2	$\overline{B}$ (kG)	F^2	$\Delta\overline{B}$ (G)	$\Delta F^2/F^2$ %
1	3.082	0.00123	3.061	0.00120	-21	-2.4
2	2.889	0.0215	2.920	0.0198	31	-7.9
3	2.932	0.0645	2.990	0.0613	58	-5.0
4	3.153	0.1203	3.219	0.1135	66	-5.7
5	3.215	0.1671	3.263	0.1612	48	-3.5
6	3.225	0.2089	3.241	0.2143	16	+2.6
7	3.269	0.2530	3.290	0.2572	21	+1.7
8	3.299	0.2871	3.299	0.2911	0	+1.4
9	3.351	0.3074	3.335	0.3096	-16	+0.7
10	3.489	0.2969	3.479	0.2958	-10	-0.4
11	3.675	0.2712	3.645	0.2767	-30	+2.0
12	3.869	0.2306	3.831	0.2399	-38	+4.0
13	4.080	0.1825	4.067	0.1876	-13	+2.8
14	4.242	0.1324	4.373	0.1035	+131	-21.8
15	4.694	0.0635	4.547	0.0860	-147	+35.4

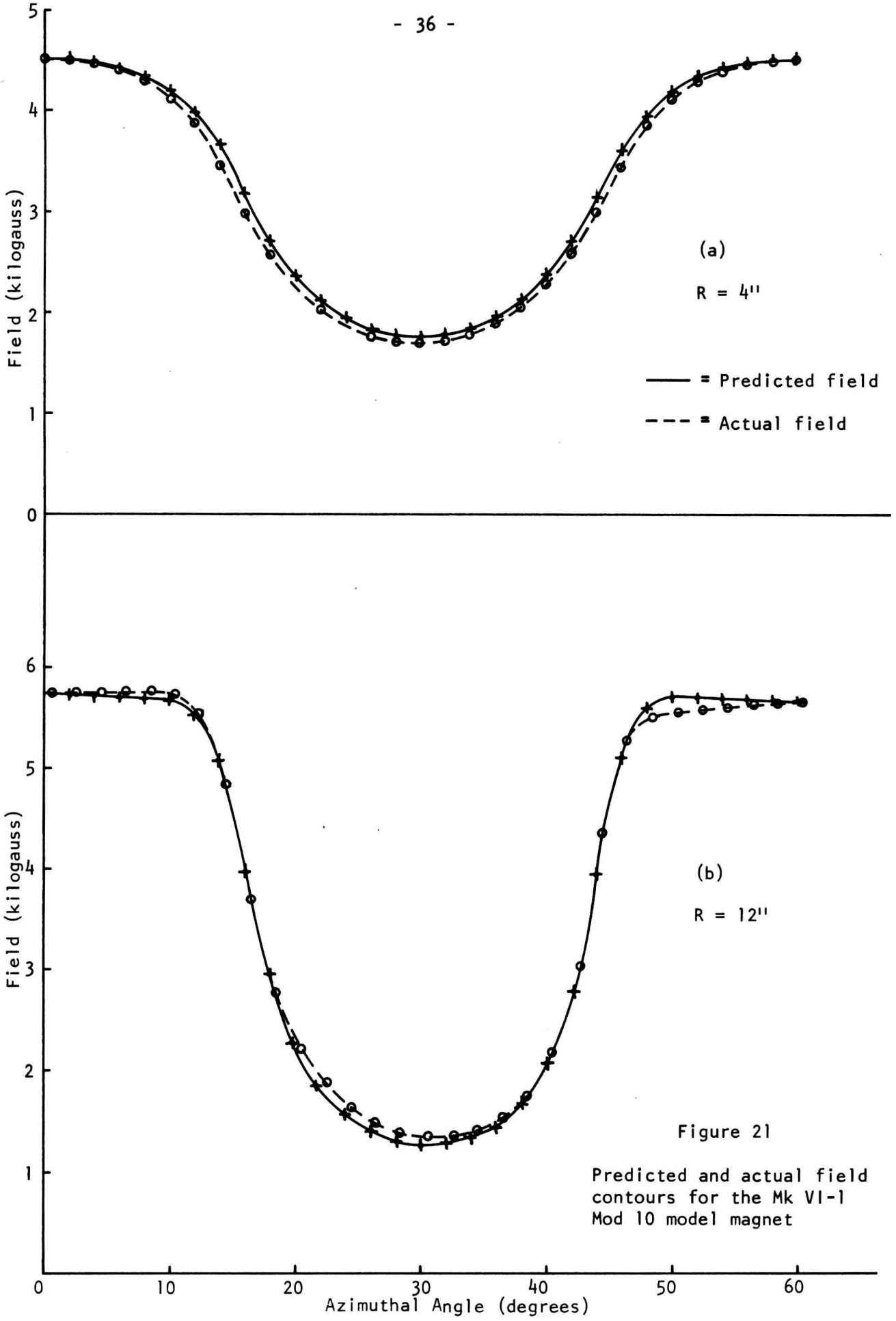

Figure 21

Predicted and actual field contours for the Mk VI-1 Mod 10 model magnet

4. TOLERANCES

4.1 Theory

The tolerances on the dimensions of the pole tip are determined from a) the isochronism condition on $\bar{B}$, and b) the requirement that vertical focusing be real and not pass through any serious resonances. The method to be used here is that of Craddock and Richardson.[7]

The equation for vertical focusing, as in Section 2.2.2, is:

$$\nu_z^2 = -\mu' + F^2(1 + 2\tan^2\varepsilon). \tag{8}$$

The limits on ν_z^2 are set from the following considerations. The lower limit is $\nu_z^2 = 0$, because ν_z, the number of betatron oscillations the particle makes per revolution, must be real. The upper limit is set by the various resonances between the vertical oscillations and either the magnet structure or the radial oscillations. The closest, most serious vertical resonance is the $\nu_z = 1/2$ resonance. Hence the upper limit is $\nu_z^2 = 0.25$. The value chosen for the TRIUMF cyclotron is $\nu_z^2 = 0.125 \pm 0.05$. The tolerance quoted allows 2.5 standard deviations in ν_z^2 before we reach either limit. Hence ν_z^2 should remain sufficiently far away from both 0 and 1/2 that the amplitude of the beam oscillations will not increase appreciably.

We wish to find the allowable errors in F^2 and ε by means of eqn.(8). The tolerance on μ' comes from the equation defining it:

$$\mu' = \frac{r}{\bar{B}}\frac{d\bar{B}}{dr}.$$

Differentiating, we find

$$\Delta\mu' = \Delta\left(\frac{r}{\bar{B}}\right)\frac{d\bar{B}}{dr} + \frac{r}{\bar{B}}\Delta\left(\frac{d\bar{B}}{dr}\right) \approx \frac{r}{\bar{B}}\Delta\left(\frac{d\bar{B}}{dr}\right) \tag{20}$$

since the permissible percentage error in $\bar{B}$ is negligible compared to that in $d\bar{B}/dr$. The tolerance on $d\bar{B}/dr$ is set to ± 2 G/ft because of trim coil considerations. Hence from eqn.(20) we can find $\Delta\mu'$ for any r and $\bar{B}$, and then from eqn.(8) we can find the allowable error in $F^2(1+2\tan^2\varepsilon)$.

This error is now broken up arbitrarily such that 95.5% of it applies to the $(1 + 2 \tan^2\varepsilon)$ term, since the spiral angle ε is the most critical parameter at large radii. This leaves 30% of the error to the F^2 term, following the rules for addition of standard deviations.

We are now able to find tolerances for F^2 and ε. We must now translate these into usable tolerances on the azimuthal positions of the focusing and defocusing edges of the pole tip. From geometry, we have

$$2 \tan \varepsilon = \tan \varepsilon_f + \tan \varepsilon_d$$

$$2\Delta \tan \varepsilon = \sqrt{(\Delta \tan \varepsilon_f)^2 + (\Delta \tan \varepsilon_d)^2} \qquad (21)$$

where ε_f and ε_d are the spiral angles of the focusing and defocusing edges, respectively. We now introduce a weighting factor λ defined by

$$\Delta \tan \varepsilon_d = \Delta\varepsilon_d/\cos^2\varepsilon_d = 2 \cos \lambda \cdot \Delta \tan \varepsilon$$

$$\Delta \tan \varepsilon_f = \Delta\varepsilon_f/\cos^2\varepsilon_f = 2 \sin \lambda \cdot \Delta \tan \varepsilon.$$

This definition of λ satisfies eqn.(21). If we assume that the work involved in shimming is inversely proportional to the angular tolerance raised to the power n, where n is normally assumed to be 1, then minimizing the total work yields

$$\tan \lambda = \left(\frac{\cos \varepsilon_d}{\cos \varepsilon_f}\right)^{\frac{2n}{2+n}} . \qquad (22)$$

From this we can find λ, and hence $\Delta\varepsilon_d$ and $\Delta\varepsilon_f$.

To find a tolerance on the azimuthal value of the measured points, we have, from geometrical considerations,

$$\Delta y_d = \frac{h'}{\sqrt{2}} \frac{\Delta\varepsilon_d}{\cos\varepsilon_d} \qquad (23)$$

where h' = distance between the measured points, and Δy_d = allowable azimutal error in the measured point. The tolerances on the points in a direction perpendicular to the tangent to the spiral can again be found from geometry to be

$$\Delta a_d = \frac{h'}{\sqrt{2}} \Delta \varepsilon_d . \qquad (24)$$

Similar equations hold for the defocusing edge of the pole tip.

We now have the necessary formulae to determine the required tolerances on the manufactured pole tip.

4.2 Results

The Mk VI-1 Mod 10 pole tip was measured with the aid of a milling edge-finder to an accuracy of ±0.002 in. on each point. A computer program was written which differentiated the smooth curve approximation to these points to find ε_d and ε_f. The pole tip tolerances were then found by the application of the formulae in the previous section. The whole program is listed in internal report TRI-I-70-4.

The calculated tolerances appear in Table II. These tolerances are beyond the contouring accuracy available in flame cutting large 10 in. thick plate steel. Therefore, the pole piece will be cut undersize, and shims will be added during assembly to achieve the correct contour.

TABLE II

TOLERANCES FOR THE MK VI-1 MOD 10 POLE TIP

R (in.)	$\Delta F^2/F^2$ (%)	$\Delta\langle(B-B)^2\rangle^{\frac{1}{2}}$ (G)	ε (deg)	ε_d (deg)	$\Delta\varepsilon_d$ (mrad)	Δa_d (in.)	Δy_d (in.)	ε_f (deg)	$\Delta\varepsilon_f$ (mrad)	Δa_f (in.)	Δy_f (in.)
50	10.7	60.6	0	0	-	-	-	0	-	-	-
100	7.9	53.3	0	0	-	-	-	0	-	-	-
150	5.3	45.3	1.0	0.2	-	-	-	1.8	-	-	-
200	3.4	34.7	18.3	24.5	118.9	0.840	0.923	11.6	131.1	0.927	0.946
250	2.0	19.8	43.0	46.9	33.0	0.233	0.341	38.4	39.6	0.280	0.357
260	1.8	16.3	50.0	53.3	25.0	0.177	0.295	46.1	30.4	0.215	0.310
270	1.6	13.2	56.4	58.7	19.1	0.135	0.260	53.7	22.8	0.161	0.272
280	1.5	10.6	62.0	61.2	16.2	0.115	0.237	62.7	15.1	0.107	0.233
290	1.3	10.0	62.7	60.3	15.0	0.106	0.214	64.7	12.3	0.087	0.203
300	1.2	9.5	63.4	62.5	12.2	0.086	0.186	64.3	11.2	0.079	0.182
305	1.1	8.4	66.1	67.6	9.06	0.064	0.168	64.4	10.7	0.076	0.176
310	1.0	6.7	70.7	74.7	5.48	0.039	0.147	63.9	10.9	0.077	0.175
311	1.0	6.2	72.0	76.4	4.75	0.034	0.142	63.8	11.0	0.078	0.176

5. FLUX CALCULATIONS

5.1 Flux Measurements

A survey of the flux in the steel return yoke of the Mk VI-1 Mod 9 model magnet was taken. A single loop of fine wire was wrapped around the steel through which the flux was to be measured. The ends of this loop were connected to a digital voltmeter (DVM) which was set to read volts integrated over time (volt-sec). The magnet power supply was run up to its full rating and back down again, with the DVM being read and reset after both the up cycle and the down cycle. The two readings were averaged to eliminate zero drift in the DVM.

The magnetic flux in the steel was then calculated by applying Faraday's Law, which states that

$$V = -\frac{d\Phi}{dt} \tag{25}$$

where V is the electromotive force induced in the coil, and Φ is the flux flowing through the area enclosed by the coil. Solving for Φ, we find

$$\Phi = -\int_0^t V d\tau \, . \tag{26}$$

The term on the right is just the DVM reading.

If we know Φ, we can find B_s, the field strength inside the steel, by using the definition of Φ:

$$\Phi \equiv \int \vec{B} \cdot \vec{n} \, da = B_n A \tag{27}$$

where B_n is the field normal to the coil, and A is the area of the coil. We then have

$$B_s = \sqrt{B_1^2 + B_2^2 + B_3^2} \tag{28}$$

where B_1, B_2 and B_3 are the field strengths at one spot in three mutually perpendicular directions.

A series of horizontal yoke radial flux measuring coils were set up, as in Figure 22. See Figure 1 for a general view of the magnet. The

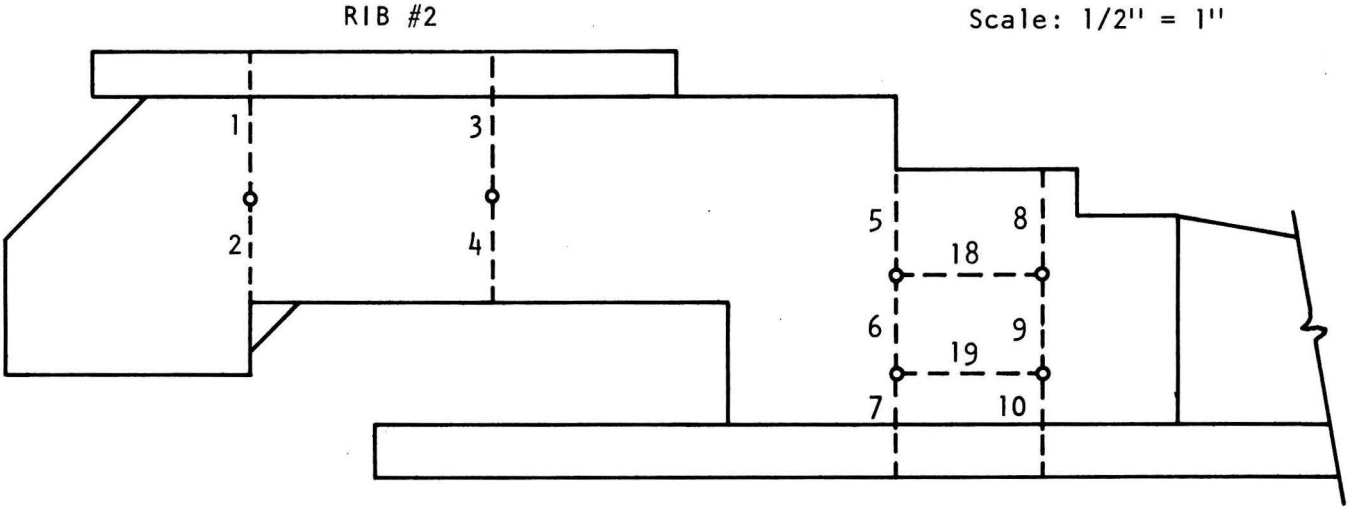

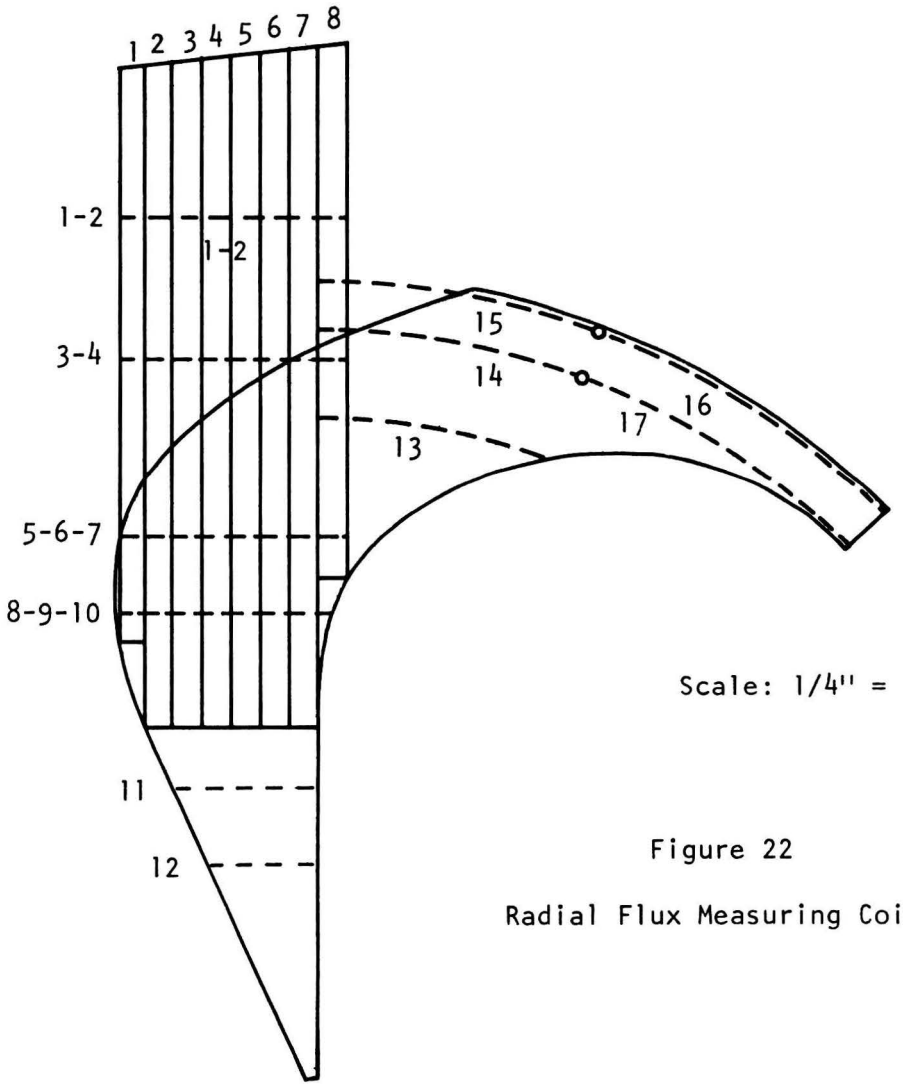

Figure 22

Radial Flux Measuring Coils

average fields inside each coil are given in Table III. All areas and radii are given in full-scale dimensions. Coils 18 and 19 show the existence of a vertical B component. Its contribution to the total field can be calculated by eqn.(28) as follows:

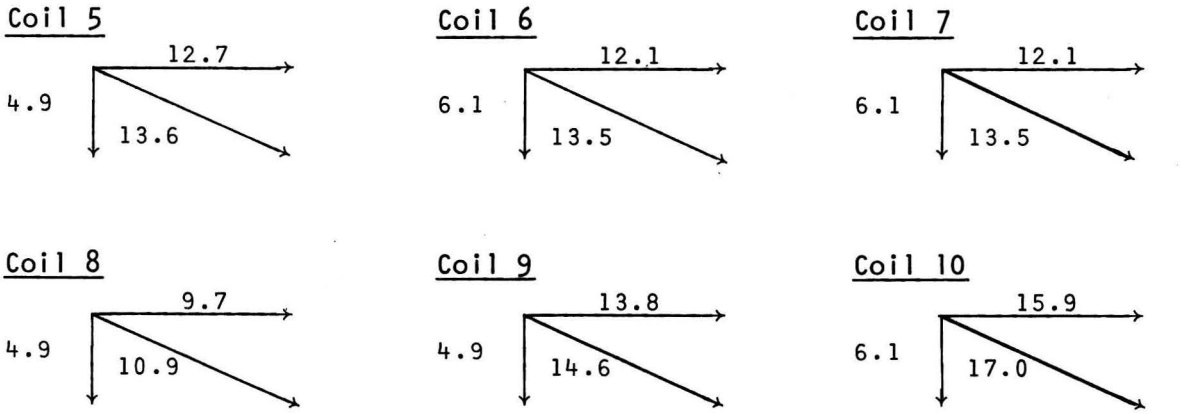

Hence the increase in $|B|$ is of the order of 10%, and must be taken into account in any permeability calculations.

Similarly, a series of vertical return yoke flux measuring coils were set up as shown in Figure 23, and the results are given in Table IV. Table V gives the results of the runs done on the eighth-scale central region model.

The coils for measuring the transverse flux in the horizontal yoke are shown in Figure 24, and the results in Table VI. As expected, coils D and E show very little transverse flux, but the lower section of coil F has a 6.1 kG average field through it. Coil H demonstrates the extremely complex nature of the flux lines in the magnet. Figure 25 is a graph of the field flowing through coil H plotted against the potentiometer setting of the magnet power supply which is a linear function of the magnet coil excitation (940 corresponds to full excitation). This behaviour is difficult to explain, but it has to do with the variation of steel permeability with changing coil induction. Figure 25 also has a similar plot for coil 16. Note the change of scale for this curve. It can be seen that the steel in this region is highly saturated, as the incremental permeability is the same as that of air.

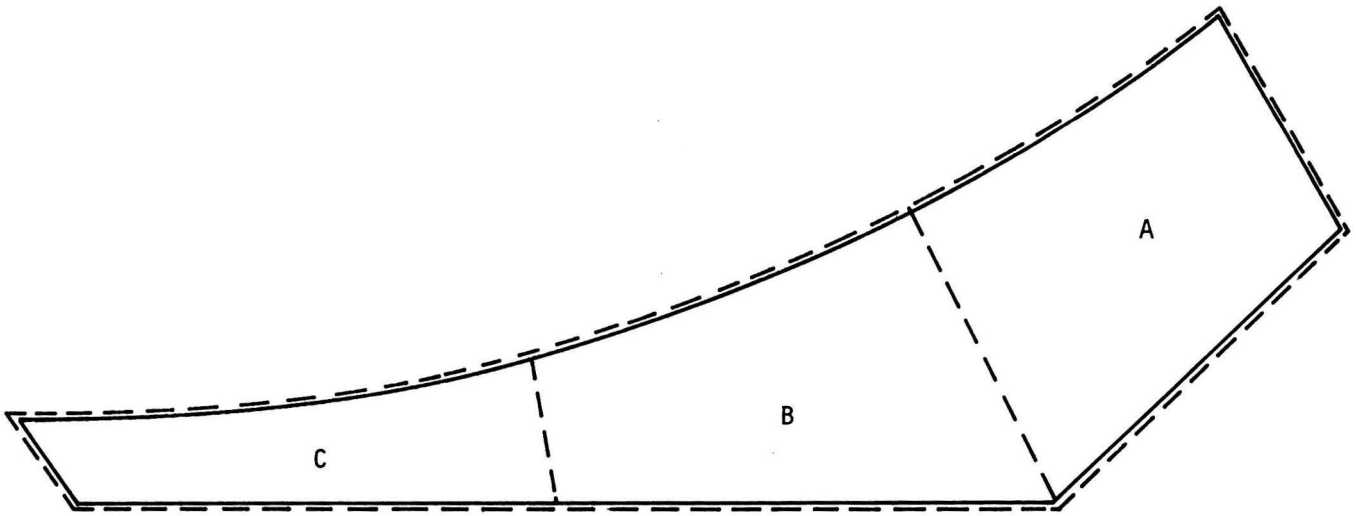

Figure 23. Vertical Return Yoke Coils

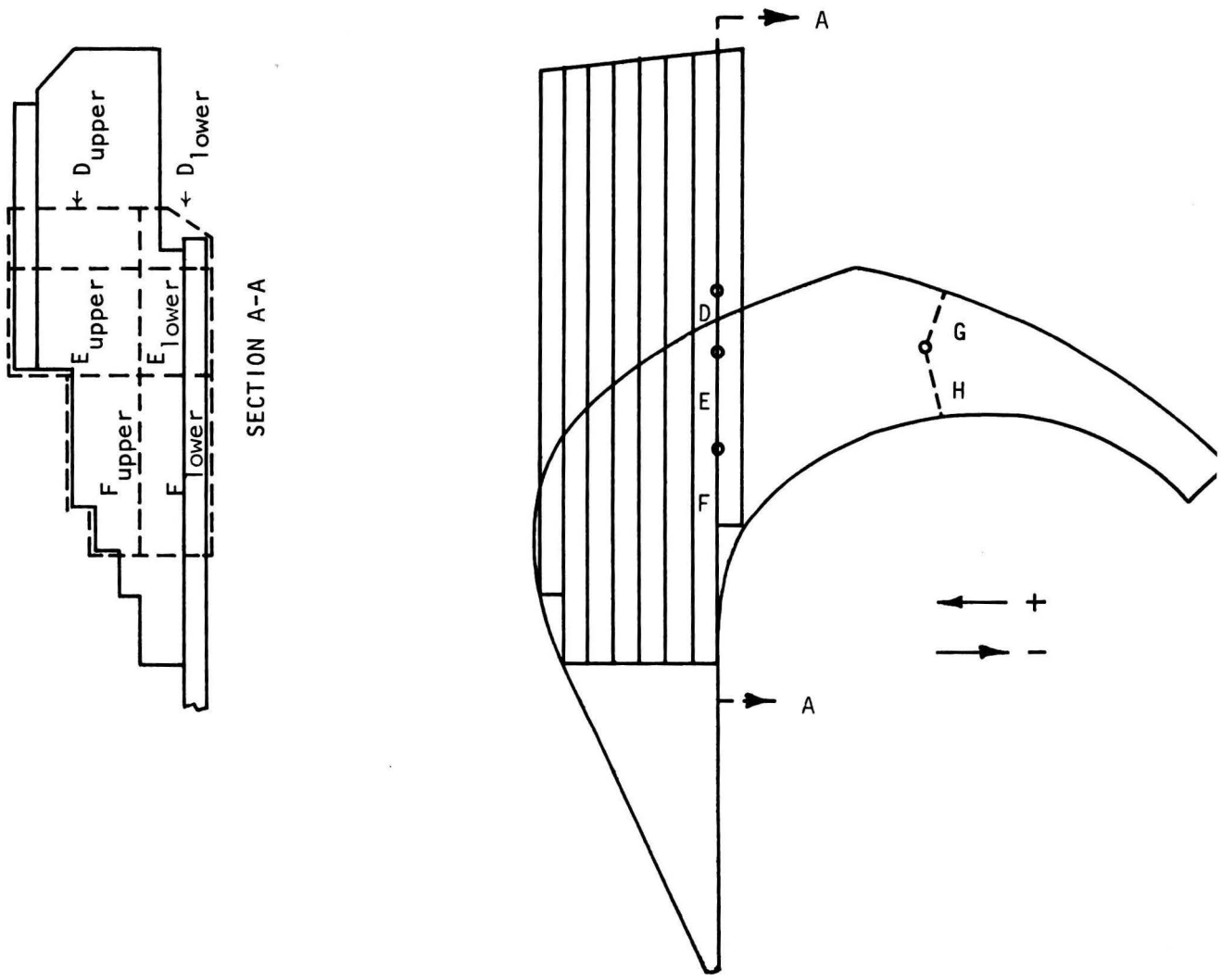

Figure 24. Transverse Coils

TABLE III - HORIZONTAL YOKE RADIAL FLUX

Coil #	Area ($in.^2$)	Approx. Radius (in.)	B (kG)	Coil #	Area ($in.^2$)	Approx. Radius (in.)	B (kG)
1	2680	354	18.1	11	2380	114	14.7
2	1790	354	22.9	12	1220	83	17.6
3	2680	312	18.9	13	1860	260	12.0
4	1790	312	22.0	14	3030	312	11.5
5	1790	218	12.7	15	1770	338	22.1
6	1950	218	12.1	16	1930	338	28.1
7	2380	218	12.1	17	2920	312	10.0
8	780	187	9.7	18	2530	-	4.9
9	1570	187	13.8	19	2600	-	6.1
10	1570	187	15.9				

TABLE IV - VERTICAL RETURN YOKE FLUX

Coil	Area ($in.^2$)	B (kG)
A	4970	17.7
B	4020	16.3
C	2620	20.3

TABLE V - CENTRE REGION FLUX

Radius (in.)	Area ($in.^2$)	B (kG)
16	25.1	20.3
24	79.4	15.6
32	105.6	19.7
36	173.4	16.1

TABLE VI - HORIZONTAL YOKE TRANSVERSE FLUX

Coil	Area ($in.^2$)	B (kG)	Coil	Area ($in.^2$)	B (kG)
D_{upper}	1280	-1.08	F_{upper}	2080	0.60
D_{lower}	805	0.14	F_{lower}	2000	6.10
D_{total}	2080	-0.66	F_{total}	4080	3.48
E_{upper}	2370	-1.48	G	813	-0.75
E_{lower}	1560	3.15	H	1460	-6.11
E_{total}	3920	0.35			

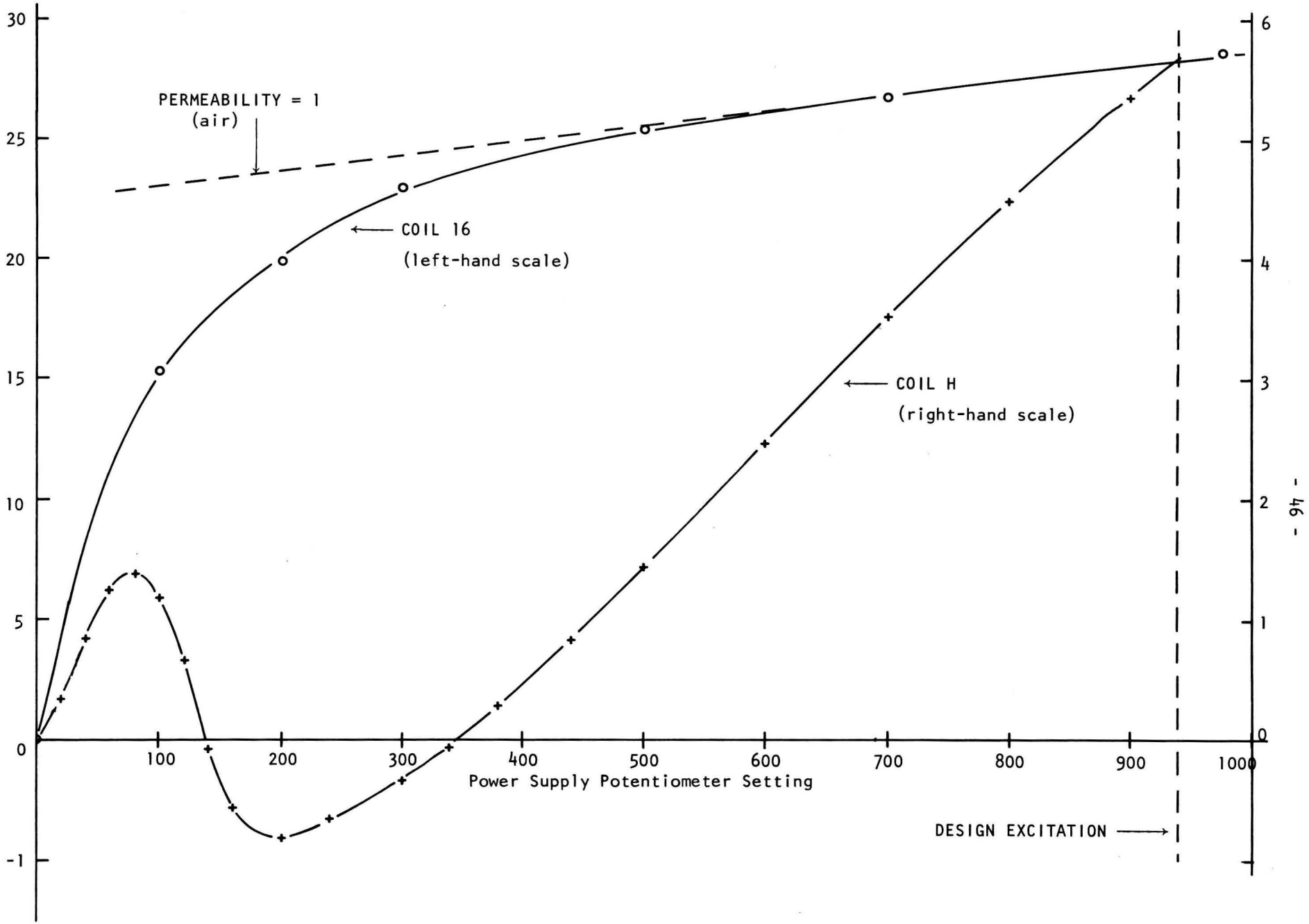

Figure 25. Field through coils H and 16 as a function of the power supply potentiometer setting, which is proportional to the main coil excitation

A small leakage flux exists around the main magnet coils. Figure 26 and Table VII show this. The leakage flux is due to the fact that the flux return path length between the coils is comparable to the magnet gap, and hence a shorting effect occurs.

TABLE VII

LEAKAGE FLUX

Coil	Area (in.^{2})	B (kG)
J	247	1.16
K	2310	0.92

5.2 Flux Calculations

Let us assume that all the flux crossing the median plane of the magnet reached that point by traversing a path through the steel return yoke. Let us also assume that the flux crossing the median plane at any radius left the steel at that same radius. We can then find the total flux Φ crossing the median plane inside radius R from

$$\Phi = 2\pi \int_0^R \overline{B}\, r\, dr. \qquad (29)$$

By our first assumption, Φ is also the flux flowing through the steel at radius R. If we know A_s', the area of the steel return yoke as a function of R, then we can use relation 27 to compute the field strength B_s in the steel. The results of this calculation for the Mk VI-1 Mod 9 model magnet are shown in Table VIII.

Table IX compares these results with the actual experimental B_s values obtained in Section 4.1. The calculated values are too big by a factor of about 1.2. Since the calculated flux crossing the median plane must be accurate to within one or two per cent, most of this discrepancy is due to flux leakage - some of the flux travels through the air rather than the steel. The ratio of the actual B_s to the calculated B_s is about 0.85; hence about 15% of the flux takes a path through the air.

5.3 Calculation of Magnet Reluctance

The calculation of the magnetic reluctance of the cyclotron magnet is a very complex problem requiring several simplifying assumptions.

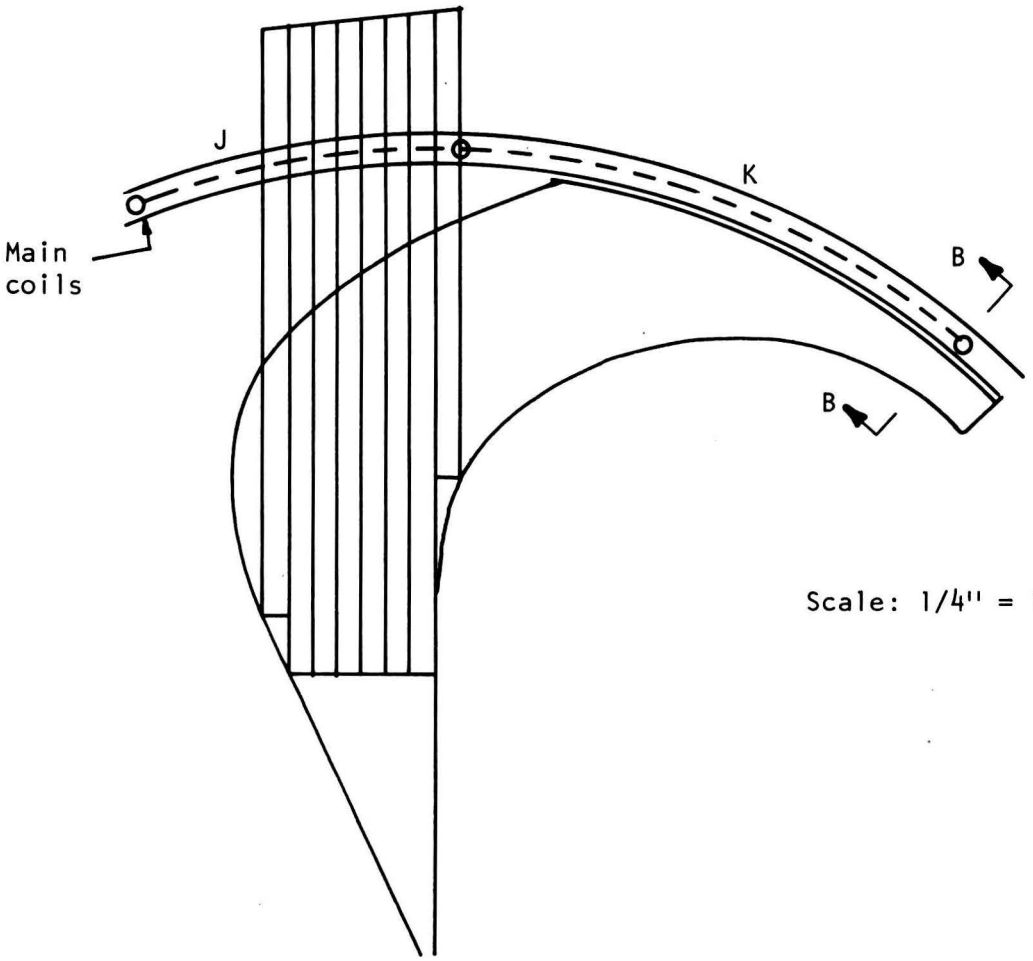

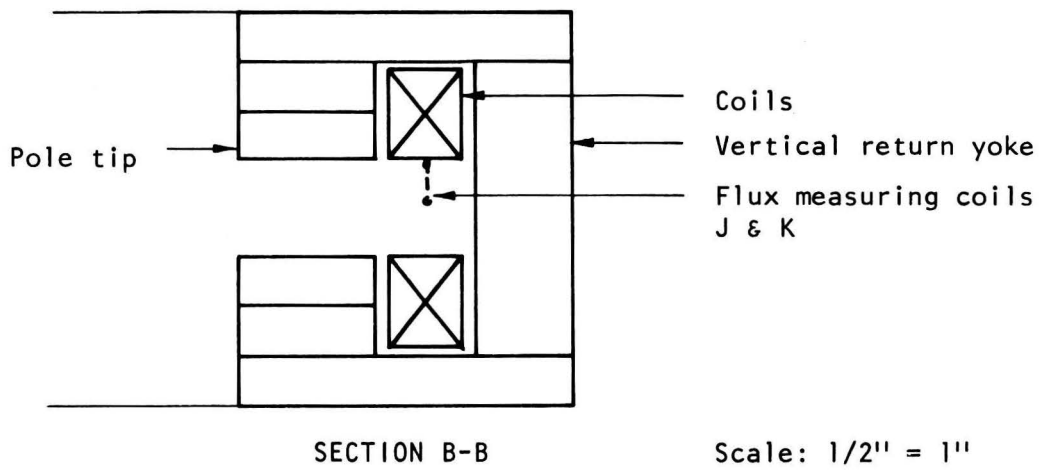

Figure 26. Leakage Flux Coils

TABLE VIII

CALCULATED FLUX DENSITY IN STEEL FOR MK VI-1 MOD 9 MAGNET

Radius (model in.)	Φ (kG-in.^{2})	A_s (in.^{2})	B_s (kG)
2	4.92	0.4	12.3
4	25.3	1.2	21.1
6	57.8	3.8	15.2
8	106.0	6.5	16.3
10	169.0	12.0	14.1
12	254.0	16.5	15.4
14	366.0	21.4	17.1
15	432.0	23.5	18.4
16.25	528.0	25.9	20.4

TABLE IX

CALCULATED FLUX DENSITIES COMPARED WITH ACTUAL FLUX DENSITIES

R (in.)	B(measured) (kG)	B(calc) (kG)	Ratio
15	14.8	18.4	0.80
10.5	12.3	14.3	0.86
9	13.8	15.9	0.87
5.5	14.7	17.5	0.84

First, let us assume a radial flux flow, with the field crossing the median plane at radius R coming from the steel at R. To a first-order approximation we can divide the magnet into N radial increments. Each increment has two components of reluctance - the steel and the gap.

$$Z = Z_s + Z_g. \tag{30}$$

The reluctance of the steel is just

$$Z_s = \frac{\ell_s}{(1 + \mu)a_s} \tag{31}$$

where ℓ_s is the effective path length through the steel (the radial increment in this case), a_s is the cross-sectional area of the steel, and μ is the steel permeability. The term $1 + \mu$ accounts for the possibility of the flux taking an air path, assuming that the length and area of the air path are the same as those for the steel flux path. The gap reluctance can be broken into two parallel components - the hill gap and the valley gap reluctances:

$$Z_g = \frac{Z_h Z_v}{Z_h + Z_v}\ , \tag{32}$$

$$Z_h = \frac{\ell_h}{a_h} = \frac{20}{a_h},\ Z_v = \frac{\ell_v}{a_v}\ . \tag{33}$$

for a given magnet, we know the hill and valley areas a_h and a_v, but we do not know the effective valley path length ℓ_v. We can estimate ℓ_v from the relationship

$$a_h Z_h\ B_h = a_v Z_v\ B_v$$

which comes from the fact that the two reluctances are in parallel. Thus we have

$$\ell_v = a_v Z_v = a_v Z_h \frac{a_h}{a_v} \frac{\overline{B}_h}{\overline{B}_v} = \ell_h \frac{\overline{B}_h}{\overline{B}_v} = 20 \frac{\overline{B}_h}{\overline{B}_v}\ . \tag{34}$$

The magnetic circuit is shown in Figure 27. Z_y is the vertical return yoke reluctance, and NI is the magnetomotive force of the main excitation coils. The total reluctance of the magnet can be calculated as follows:

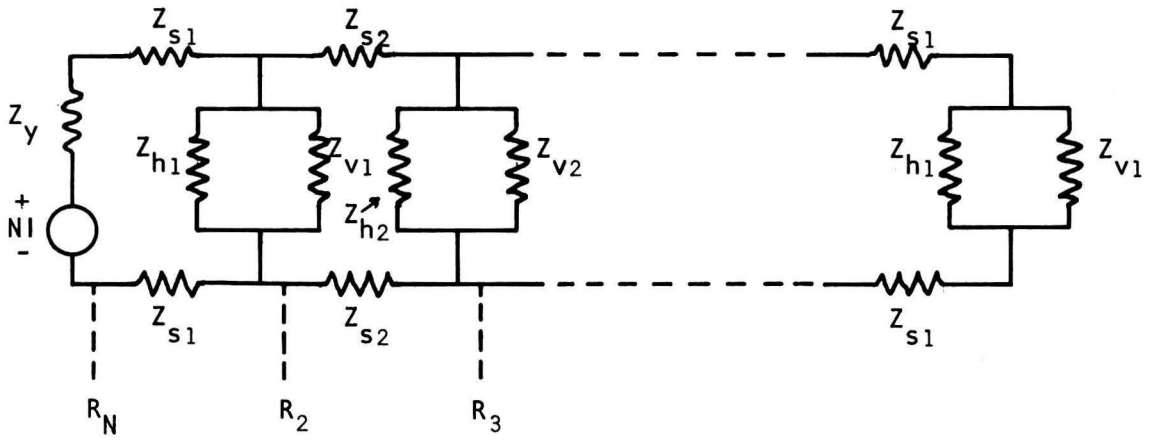

Figure 27. Magnetic Circuit of TRIUMF Magnet

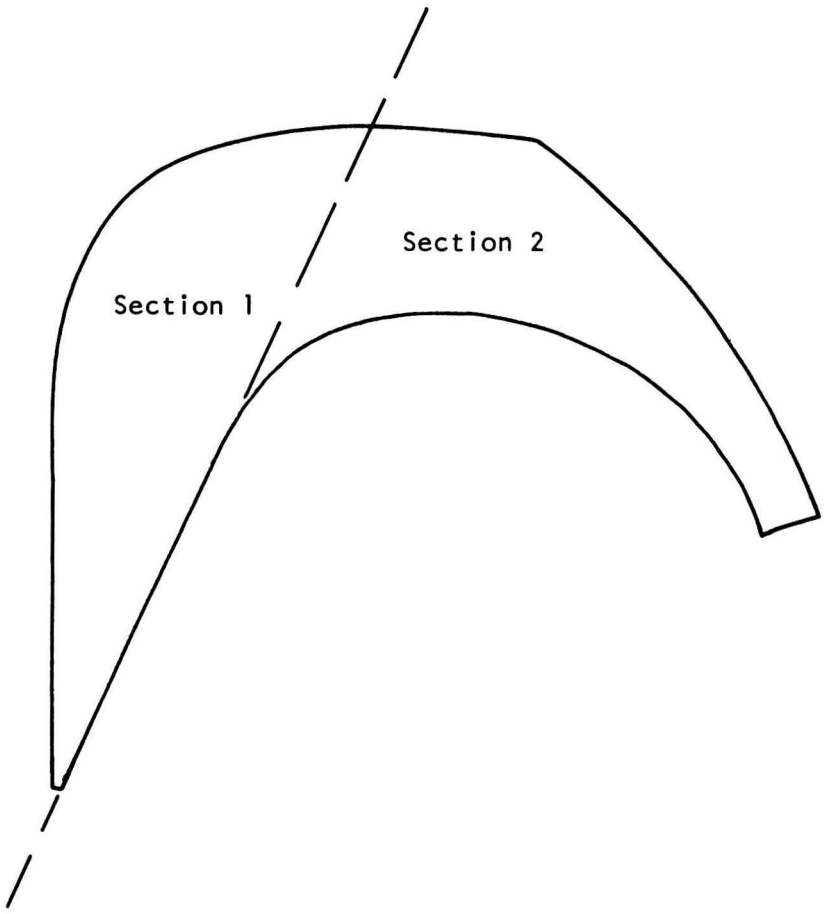

Figure 28. Division of Pole Tip used for Two-section Flux Calculations

$$Z_1 = 2Z_{s_1} + \frac{Z_{h_1} Z_{v_2}}{Z_{h_1} + Z_{v_1}}$$

$$Z_2 = 2Z_{s_2} + \frac{Z_{h_2} Z_{v_2} Z_1}{Z_{h_2} Z_{v_2} + Z_1 (Z_{h_2} + Z_{v_2})} . \qquad (35)$$

This process is repeated until Z_n has been computed. Then the total reluctance is

$$Z_t = Z_n + Z_y . \qquad (36)$$

Z_t can be used to calculated NI, via the relationship

$$NI = \frac{1}{0.4\pi} \Phi \, Z_t . \qquad (37)$$

The calculation was carried out on the Mk VI-1 Mod 9 model magnet. The program used for this is listed in Int. Rep. I-70-4. The results were not encouraging. The calculated number of ampere-turns required was 15,800, but the actual number is 33,650. One of the major causes of this discrepancy was the assumption implicit in the calculation that all the steel at any particular radius has the same permeability. The flux measurements in Section 5.1 show how bad an assumption this is. However, a calculation which takes this factor into account would be very difficult. A partial correction can be done by dividing the magnet azimuthally into two sections, calculating the reluctance for each section, and adding them in parallel. The natural division is along the line shown in Figure 28, as the height of the steel return yoke suddenly changes here. Also, since the return yoke plates are along a radius line, the air gaps between the plates will tend to prevent flux going from one section to the other. The flux measurements do tend to vindicate this approximation. This calculation was also performed using the Mk VI-1 Mod 9 data, and resulted in an excitation of 25,500 ampere-turns.

There are many major sources of error in a calculation of this type. For one thing, the steel permeability is very strongly dependent on the field strength - a small ΔB_s results in a large $\Delta\mu$. The calculations assume that μ is constant over the whole steel cross-section, but

this far from reality. The computed path lengths in the steel are also wrong, as the flux does not necessarily travel radially. Air leakage flux must produce some discrepancy. The two-section calculation does not allow any flux leakage from one section to the other, which is also not true. In general, then, the very complex geometrical shape of the TRIUMF magnet will make any fairly simple reluctance calculations accurate to only ±25% or so.

The method described here is accurate enough for tolerance calculations, however. When the two-section calculation above was redone with the steel permeability changed by 10%, it was found that the magnet reluctance changed by 4%. Adding on 25% for the error in the calculation gives a maximum reluctance change of 5%. So we have

$$\frac{\Delta\mu}{\mu} \simeq 2\,\frac{\Delta z}{z}\,. \tag{38}$$

We can compare this with the results obtained by Craddock and Richardson.[7] Since $\frac{\Delta z}{z} \simeq \frac{1}{200}$ for TRIUMF, then by eqn.(38),

$$\frac{\Delta\mu}{\mu} \simeq \frac{1}{100}\,. \tag{39}$$

This corresponds closely with Craddock and Richardson's result of

$$\frac{\Delta\mu}{\mu} \simeq \frac{1}{150}\,.$$

ACKNOWLEDGEMENTS

I should like to thank Dr. E.G. Auld for his many helpful suggestions, and also for his continual optimism and encouragement, without which this thesis might never have been completed.

I should also like to thank Dr. G. Mackenzie, Dr. M. Craddock and Mr. A. Otter for their suggestions and improvements, and Ada Strathdee, Paul van Rook, and the rest of the TRIUMF staff for their invaluable help.

REFERENCES

1. J. Reginald Richardson, Sector-Focusing Cyclotrons, *Progress in Nuclear Techniques and Instrumentation* (North-Holland, Amsterdam, 1965), 1, 1-101
2. L. Smith and A.A. Garren, Orbit Dynamics in the Spiral-Ridged Cyclotron, UCRL 8598 (1959)
3. T.I. Arnette, H.G. Blosser, M.M. Gordon and D.A. Johnson, Cyclotron Programs for a Small Computer, Nucl. Instr. Meth. 18,19, 343 (1962)
4. M.K. Craddock and V.J. Harwood, private communication (1968)
5. B.C. Mullen, Toward an Accurate Calculation of the Mean Lifetime of the H^- Ion in an Electric Field, M.Sc. Thesis, Department of Physics, University of British Columbia (1968)
6. G.M. Stinson, W.C. Olsen, W.J. McDonald, P. Ford, D. Axen and E.W. Blackmore, Electric Dissociation of H^- Ions by Magnetic Fields, TRI-69-1 (1969)
7. M.K. Craddock and J. Reginald Richardson, Magnetic Field Tolerances for a Six-Sector 500 MeV H^- Cyclotron, TRI-67-2 (1968)
8. J.J. Livingood, *Principles of Cyclic Particle Accelerators* (D. van Nostrand Co., Inc., Princeton, New Jersey, 1961)
9. E.G. Auld, J.J. Burgerjon and M.K. Craddock, Initial Model Magnet Study for a Six-Sector 500 MeV H^- Cyclotron, TRI-67-1 (1967)
10. W. Walkinshaw and N.M. King, Linear Dynamics in Spiral Ridge Cyclotron Design, AERE GP/R 2050 (1956)
11. K.R. Symen, D.W. Kerst, L.W. Jones, L.J. Laslett, and K.M. Terwilliger, Fixed Field Alternating Gradient Particle Accelerators, Phys. Rev. 103, 1837 (1956)
12. J.R. Hiskes, unpublished, quoted in D.L. Judd, Nucl. Instr. Meth. 18,19, 70 (1962)